

1974

Measurements of the magnetic dipole moments of the antiproton and the sigma- hyperon

B. Lee Roberts

College of William & Mary - Arts & Sciences

Follow this and additional works at: <https://scholarworks.wm.edu/etd>



Part of the [Physics Commons](#)

Recommended Citation

Roberts, B. Lee, "Measurements of the magnetic dipole moments of the antiproton and the sigma-hyperon" (1974). *Dissertations, Theses, and Masters Projects*. Paper 1539623674.

<https://dx.doi.org/doi:10.21220/s2-3j14-x488>

This Dissertation is brought to you for free and open access by the Theses, Dissertations, & Master Projects at W&M ScholarWorks. It has been accepted for inclusion in Dissertations, Theses, and Masters Projects by an authorized administrator of W&M ScholarWorks. For more information, please contact scholarworks@wm.edu.

INFORMATION TO USERS

This material was produced from a microfilm copy of the original document. While the most advanced technological means to photograph and reproduce this document have been used, the quality is heavily dependent upon the quality of the original submitted.

The following explanation of techniques is provided to help you understand markings or patterns which may appear on this reproduction.

1. The sign or "target" for pages apparently lacking from the document photographed is "Missing Page(s)". If it was possible to obtain the missing page(s) or section, they are spliced into the film along with adjacent pages. This may have necessitated cutting thru an image and duplicating adjacent pages to insure you complete continuity.
2. When an image on the film is obliterated with a large round black mark, it is an indication that the photographer suspected that the copy may have moved during exposure and thus cause a blurred image. You will find a good image of the page in the adjacent frame.
3. When a map, drawing or chart, etc., was part of the material being photographed the photographer followed a definite method in "sectioning" the material. It is customary to begin photoing at the upper left hand corner of a large sheet and to continue photoing from left to right in equal sections with a small overlap. If necessary, sectioning is continued again -- beginning below the first row and continuing on until complete.
4. The majority of users indicate that the textual content is of greatest value, however, a somewhat higher quality reproduction could be made from "photographs" if essential to the understanding of the dissertation. Silver prints of "photographs" may be ordered at additional charge by writing the Order Department, giving the catalog number, title, author and specific pages you wish reproduced.
5. PLEASE NOTE: Some pages may have indistinct print. Filmed as received.

Xerox University Microfilms

300 North Zeeb Road
Ann Arbor, Michigan 48106

74-22,288

ROBERTS, Bradley Lee, 1946-
MEASUREMENTS OF THE MAGNETIC DIPOLE MOMENTS OF THE
ANTIPROTON AND THE Σ^- HYPERON.

The College of William and Mary in Virginia,
Ph.D., 1974
Physics, elementary particles

University Microfilms, A XEROX Company, Ann Arbor, Michigan

MEASUREMENTS OF THE MAGNETIC DIPOLE MOMENTS
OF THE ANTIPROTON AND THE Σ^- HYPERON

A Dissertation

Presented to

The Faculty of the Department of Physics
The College of William and Mary in Virginia

In Partial Fulfillment
Of the Requirements for the Degree of
Doctor of Philosophy

by

Bradley Lee Roberts

June 1974

APPROVAL SHEET

This dissertation is submitted in partial fulfillment of
the requirements for the degree of

Doctor of Philosophy

Bradley Lee Roberts
Author

Approved, May 1974

Robert E. Welsh
Robert E. Welsh

Morton Eckhause
Morton Eckhause

John R. Kane
John R. Kane

Rolf G. Winter
Rolf G. Winter

Hans C. von Baeyer
Hans C. von Baeyer

Kelly G. Shaver
Kelly G. Shaver
Department of Psychology

MEASUREMENTS OF THE MAGNETIC DIPOLE MOMENTS

OF THE ANTIPROTON AND THE Σ^- HYPERON

TABLE OF CONTENTS

| | Page |
|---|------|
| ABSTRACT | v |
| I. INTRODUCTION | 1 |
| II. THEORETICAL CONSIDERATIONS | 6 |
| A. Magnetic Moments | 6 |
| B. Atomic Effects | 7 |
| III. EXPERIMENTAL PROCEDURE AND DETAILS | 14 |
| A. Introduction | 14 |
| B. Beam Description | 14 |
| C. Counter Arrangement and Electronic Logic | 16 |
| D. X Ray Detection | 17 |
| E. Fast-Slow Timing | 19 |
| F. Energy Calibration and Stabilization | 20 |
| G. Targets | 22 |
| IV. DATA ANALYSIS | 23 |
| A. Calibration Analysis | 23 |
| B. Analysis for Fine-Structure Splitting | 24 |
| C. Data Simulation | 29 |
| V. RESULTS AND CONCLUSIONS | 31 |
| A. Noncircular Transitions | 31 |
| B. Instrumental Width Uncertainties | 32 |

| | | |
|-------|---|----|
| C. | Statistical Population of Fine-Structure Levels | 33 |
| D. | Dependence of Results on Region of Fit | 34 |
| E. | The Antiproton Magnetic Moment | 34 |
| F. | The Σ^- Magnetic Moment | 36 |
| VI. | TABLES | 38 |
| VII. | ACKNOWLEDGMENTS | 40 |
| VIII. | REFERENCES | 43 |
| IX. | FIGURE CAPTIONS | 48 |

ABSTRACT

The fine-structure splittings in atoms formed by antiprotons in lead and uranium and Σ^- hyperons in lead and platinum have been measured. Since the fine structure is produced through the interaction of the magnetic dipole moment of the antiproton or the Σ^- hyperon with the Coulomb field of the nucleus, a value for the magnetic moment can be determined from the splitting. The magnetic moment obtained for the antiproton was (-2.819 ± 0.056) nuclear magnetons which agrees well with the CPT prediction of -2.793 nuclear magnetons. The magnetic moment derived for the Σ^- hyperon was (-1.48 ± 0.37) nuclear magnetons which is in agreement with the sign given by simple SU(3) theory, but differs somewhat from the value of -0.9 nuclear magnetons predicted by the theory with no mass breaking.

BRADLEY LEE ROBERTS

DEPARTMENT OF PHYSICS

THE COLLEGE OF WILLIAM AND MARY IN VIRGINIA

I. INTRODUCTION

Since the first predictions of the existence of mesic atoms by Fermi, Teller, Weisskopf and Wheeler¹⁻³ and the earliest experiments which confirmed them,⁴⁻⁶ a new area of physics has developed. The subject of this field, which was first referred to as mesic atoms and more recently as exotic atoms, can be defined as systems composed of a negatively charged elementary particle bound to a positive nucleus by the Coulomb field. With the development of high energy proton accelerators a number of exotic negative particles have become available with which to form such atoms. All of these atoms have common characteristics which we will briefly discuss.

Exotic atoms are analogous, in many respects, to a hydrogen atom but with a nucleus of charge Ze and mass A . Their basic properties can be obtained by examining the Bohr formulae for the energy and radius of a particle of mass M in orbit about a nucleus of mass M_N , charge Ze and principal quantum number n .

$$\text{Bohr Radius: } r_n = \frac{n^2}{mZ\alpha}$$

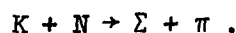
$$\text{Bohr Energy: } E_n = - \frac{m(Z\alpha)^2}{2n^2} = - 1/2 \frac{Z\alpha}{r_n}$$

where m is the reduced mass, $m = MM_N/(M + M_N)$, and $\alpha = e^2/\hbar c$ is the fine-structure constant. One notes that for $M_N \gg M$, $m \approx M$ and the Bohr radius

is then inversely proportional to the mass of the orbiting particle. Thus for any particle heavier than an electron the lower Bohr orbits are well inside the electron cloud (the muon is the lightest of the exotic particles, $m_{\mu}/m_e = 206.8$) and the effects of the electron screening become vanishingly small for low n . Exotic atoms have the property that as the atomic number increases, the $1s$ wave function probability density inside the nuclear surface increases. For negative muons, which interact weakly and electromagnetically with nucleons, this can bring about a deviation from the simple Bohr energy formula as large as 50% because the point nucleus approximation is not valid. In the case of hadrons, which additionally interact strongly with nuclear matter, strong absorption occurs from atomic states near the nucleus, and indeed for π^- mesons and the heavier hadrons the atomic cascade toward the ground state is terminated before the $1s$ state is reached.

The experimental procedure used to form an exotic atom with a long lived particle, consists of stopping a secondary beam from an accelerator in a target of the desired element. The negative particle is then captured into orbits about the target nuclei, first perhaps in molecular orbits and then atomic ones of high n , in the order of 10^{-9} to 10^{-10} seconds.^{2,7-9} The particle then cascades through the atomic levels first by the Auger process and then at lower n by electric dipole radiative transitions. Because of the time necessary to form an exotic atom, only a few particles lend themselves to direct production of exotic atoms from an accelerator beam because of the large fraction lost to decay if the

particle lifetime is too short. Experimentally, muonic, pionic, kaonic and antiprotonic atoms have been produced directly, and Σ^- atoms have been observed by production from stopping K^- . Approximately 5 - 10% of the K^- stopping in a target will produce Σ^- atoms¹⁰ by the reaction



Some of the resulting Σ^- escape from the nucleus where they were produced and form Σ^- atoms about other target nuclei. Pionic atoms are sometimes formed by the π^- produced with the above reaction so that in kaonic x-ray spectra both Σ^- and π^- x rays are present but with a much lower intensity than the K^- x rays. Wiegand¹¹ reported the first observations of Σ^- x rays. However, he observed a single x ray and no other member of the cascade. Backenstoss et al.¹² first reported the observation of several members of a cascade in low Z elements and Lam et al.¹³ reported the first observation in high Z targets.

Complete reviews of the field of exotic atoms are available in recent articles by Ericson,¹⁴ Backenstoss,¹⁵ and Wu¹⁶ which treat π^- , K^- , \bar{p} and Σ^- atoms. Those by Wu,¹⁷ Wu and Wilets,¹⁸ Devons and Duerdoth¹⁹ discuss μ^- atoms and an earlier review by West²⁰ treats μ^- and π^- atoms.

The behavior of atomic systems must be described by a relativistic wave equation, viz. the Dirac or Klein Gordon equation, depending on the spin of the orbiting particle. In either case, the energy solution, to the lowest order in α , is

$$E_{nj} = -m \frac{(Z\alpha)^2}{2n^2} \left\{ 1 + \left(\frac{Z\alpha}{n} \right)^2 \left(\frac{n}{j+1/2} - 3/4 \right) + \dots \right\}$$

where $j = \ell$ if the particle is a boson and $j = \ell \pm 1/2$ for a fermion. To this equation one must add the effects of vacuum polarization, finite nuclear size, nuclear polarization and other corrections.

The study of exotic atoms furnishes information about a number of phenomena which can be divided into three areas: the particle, the interaction and the nucleus. Particle properties are best studied by observing high n transitions in high Z elements where the x-ray energy is of the order of hundreds of KeV but the particle is sufficiently distant from the nucleus so that strong interaction and finite size effects are negligible. Owing to the short range nature of the strong force, information on the strong interaction can best be gained from those last observed transitions when the cascade is terminated by strong absorption. Quantum electrodynamic effects such as vacuum polarization are best studied using muons. In nuclear muon capture the weak interaction can be studied. Nuclear charge distributions have been determined using μ^- atoms.²¹ The nuclear mass distribution or a possible difference in neutron-proton distributions may also be studied using hadronic atoms as recently reported by Bugg, et al.²² Because pion capture occurs on nucleon pairs, π^- atoms provide information on nuclear correlations in nuclei as well as the pion-nucleus interaction.²³ The kaon-nucleus interaction²⁴ and antiproton-nucleus interaction²⁵ have been studied using exotic atoms.

Since the x-ray transition energies are proportional to the particle's mass, careful measurement of x-ray transition energies will yield a direct measurement of the mass. The best values of the μ^- , π^- , K^- , and \bar{p} masses have been obtained from exotic atom experiments.²⁶⁻²⁹

If the orbiting particle has spin $1/2$, then the levels will be doublets and a measurement of the fine-structure splitting will yield the magnetic dipole moment. In the experiments reported here, such measurements were performed to obtain the magnetic moment of the antiproton and the Σ^- hyperon. Preliminary results have already been reported.^{30,31} In the following sections the theoretical considerations, experimental procedure, and methods of data analysis are discussed. The results of analysis and conclusions drawn from them are presented in the final section.

II. THEORETICAL CONSIDERATIONS

A. Magnetic Moments

The value of the magnetic dipole moment of the antiproton is clearly predicted theoretically. The CPT theorem requires that particle-antiparticle pairs have magnetic moments equal in magnitude and opposite in sign.³² Since the CPT theorem is known to hold to a very high accuracy,³³ an experimental determination of the magnitude of the \bar{p} magnetic moment and of its sign can therefore be viewed as a stringent test of the experimental and analytical techniques used to determine the Σ^- magnetic moment.

The Σ^- magnetic moment is somewhat less clearly related theoretically to previously measured magnetic moments. It can be related to the magnetic moments of the other members of the baryon octet by SU(3) symmetry,³⁴⁻³⁶ and in fact a high precision measurement of the Σ^- moment would furnish a useful test of SU(3) theory. The difficulty of correctly including the strong interactions in the dynamics of the problem exists,³⁴ but SU(3) with no mass breaking predicts³⁵

$$\mu(\Xi^-) = \mu(\Sigma^-) = -[\mu(p) + \mu(n)]. \quad (1)$$

Furthermore SU(6), or a model with equal mass quarks predicts³⁶

$$\frac{\mu(p)}{\mu(n)} = -3/2 .$$

Thus

$$\begin{aligned}\mu(\Sigma^-) &= -1/3 \mu(p) \\ \mu(\Sigma^-) &= -0.9 \mu_N\end{aligned}\tag{2}$$

where $\mu_N = e\hbar/2m_p c$, one nuclear magneton. The possibility that the strange quark has a mass which is different from the isodoublet members has been considered by Rubinstein et al.³⁶

B. Atomic Effects

If the orbiting hadron in an exotic atom has spin 1/2, the atomic energy levels will exhibit fine-structure splitting. The magnetic moment can be decomposed into two components,³⁷

$$\mu = (g_0 + g_1)\mu_H$$

where g_0 is the Dirac factor (equal to the particle charge, +1, -1 or 0) and g_1 is the Pauli or anomalous term. Both components are expressed in units of the appropriate hadron magneton, $\mu_H = e\hbar/2m_H c$, where m_H is the hadron mass. The fine-structure splitting of an atomic level with principal quantum number n and orbital angular momentum quantum number ℓ is given by:³⁷

$$\Delta E_{n,\ell} = (g_0 + 2g_1) \frac{(\alpha Z)^4}{2n^3} \frac{m}{\ell(\ell+1)}\tag{3}$$

where Z is the nuclear charge, m the reduced mass of the hadron-nucleus system, and α is the fine-structure constant. For $\mu < 0$, the state of larger j is higher in energy. One should note that Eq. (3) was derived

in the Pauli approximation³⁷ and is accurate up to (and including) terms of relative order $(\bar{v}/c)^2$, where \bar{v} is the expectation value of the hadron velocity. The neglected terms are of relative order $(\bar{v}/c)^4$ and higher. Since $\bar{v}/c \approx Z\alpha/n$, we can see that for $n = 10$, the lowest state considered in this work, the contribution of the neglected terms is of the order of 10^{-5} below those discussed here.

If one considers atomic transitions between two fine-structure doublets, shown schematically in Fig. 1, several results are apparent. The transition from j_4 to j_1 is of negligible intensity because $\Delta j = 2$. If one assumes a statistical population of the levels, the intensity ratio for transitions a:b:c can be calculated³⁷ and is given by the expression,

$$a = \frac{1 + \frac{2j_1 + 1}{2j_2 + 1}}{\frac{2j_3 + 1}{2j_4 + 1} - \frac{2j_1 + 1}{2j_2 + 1}}$$

$$b \equiv 1 \tag{4a}$$

$$c = a \left(\frac{2j_3 + 1}{2j_4 + 1} \right) - 1 .$$

If we define circular transitions as those between levels with $\ell = n - 1$ and noncircular transitions as those between levels with $\ell \leq n - 2$, then for circular transitions and the first noncircular transitions ($\ell = n - 2$)

$$\begin{array}{ll} \text{Circular:} & a = 2n^2 + n - 1 \\ & c = 2n^2 - n - 1 \\ \text{Noncircular:} & a = 2n^2 - 3n \\ & c = 2n^2 - 5n + 2 \end{array} \tag{4b}$$

where n is the principal quantum number of the final state. For large n , the contribution of transition b can be neglected and one observes experimentally two lines, a and c , which are separated in energy by an amount δE given by

$$\delta E = \Delta E_{n,\ell} - \Delta E_{n',\ell'} \quad (5)$$

Therefore a measurement of the splitting of the two components a and c , yields a direct measurement of the magnitude of the magnetic moment. Since the intensity ratio, $R = a/c$, is not unity, it is also possible to determine the sign of the magnetic moment by a measurement of the intensity ratio.

There are several effects whose contributions must be taken into account in an analysis for fine-structure splitting. Noncircular transitions can contribute to the observed lineshape. Dynamic quadrupole mixing can modify the energy levels. Changes in the level populations may occur due to Auger transitions. These will be considered in order.

Figure 2-2 shows schematically a circular transition and the most intense noncircular one with a competing $\Delta n = 2$ transition. From Eq. (3) one sees that the splitting of the noncircular transition labelled α is greater than that of the circular one, γ . However, the energies of α and γ are not experimentally resolved, and therefore one should include the contribution from α in an analysis for fine structure splitting. The contribution due to the presence of noncircular transitions can be estimated in two different ways: an estimate based on a cascade calculation, or a direct determination from the experimental data. Only for the

analysis of the $\Sigma^-(n = 12 \rightarrow n = 11)$ x ray and the higher antiprotonic x rays was this possible.

To estimate the contribution of noncircular transitions to the observed \bar{p} -Pb and \bar{p} -U x rays, a cascade calculation similar to those described by Sapp³⁸ was performed. Only the first noncircular transition was included in the analysis for fine-structure splitting. The other noncircular transitions were much less intense and were experimentally resolved in energy from the circular and first noncircular transitions.

For the $\Sigma(12 \rightarrow 11)$ in Pb, it was possible to estimate experimentally the contribution due to the transition called α . The intensity ratio α/β is easily calculated for electric dipole radiation, and $\beta/(\alpha + \gamma)$ can be measured (or an upper limit placed on it) from the experimental data because β and γ are clearly resolved in energy. Since the $\Sigma(11 \rightarrow 10)$ was observed in Pb, the $\Sigma(12 \rightarrow 10)$ should not be so broadened by the strong interaction effects as to be unobservable. The intensity ratio $G = \alpha/\gamma$ can be determined from the intensity ratio I , where

$$I = \frac{\alpha}{\alpha + \gamma} = \frac{\beta}{\alpha + \gamma} \frac{\alpha}{\beta} .$$

For the $\Sigma^-(12 \rightarrow 11)$ in Pb we found an upper limit on $\beta/(\alpha + \gamma)$ of 0.07. The intensity ratio α/β calculated for electric dipole radiation is 2.3 for the $\Sigma^-(12 \rightarrow 11)$ in Pb. We then obtain the result:

$$I \leq .16.$$

For the \bar{p} -U system the effects of dynamic quadrupole mixing must be considered. The Hamiltonian for the hadron-nucleus system is composed

of three parts, H_N which operates only on the dynamical variables of the nucleus, H_H which operates only on the variables of the hadron (the hadron-atomic Hamiltonian) and H_{HN} which represents the hadron-nucleus interaction and which operates on both sets of variables. The total Hamiltonian of the system is given by

$$\mathcal{H} = H_N + H_H + H_{HN}$$

We have thus far ignored the term H_{HN} which has the ability to mix nuclear and hadronic states. The most important example in this work of an interaction which mixes the nuclear and hadronic states is dynamic quadrupole mixing. This is important in deformed nuclei and therefore must be included in any analysis of the \bar{p} -U x-ray spectra. This dynamic E2 effect was first treated theoretically by Willets³⁹ and Jacobsohn⁴⁰ for muonic atoms, and a more complete treatment has been carried out by Chen.⁴¹ When the off-diagonal matrix elements of the quadrupole interaction reach a value comparable in magnitude with the excitation energy of the first excited nuclear state, then the contribution of the dynamic E2 interaction becomes non-negligible and a shift in energy occurs. Shifts in K^- , \bar{p} and Σ^- energy levels in ^{238}U have been calculated by Ara and Chen,⁴² and observed by Cheng, et al.,⁴³ as well as in the present work. An absolute shift of both components of a fine-structure doublet does not affect a measurement of the magnetic moment. However, the E2 interaction mixes the states such that the new set of eigenstates are linear combinations of the states coupled by the interaction and j is no longer a good quantum number.

Calculations were made using only the first excited state of ^{238}U and the formalism developed by Chen,⁴¹ which showed that the two fine-structure components of the $n = 10, \ell = 9$ doublet were shifted equally to within 20 eV, a difference which is far less than the experimental accuracy. The calculated shifts agreed well with the more complete calculation of Chen.⁴² For the $n = 10, \ell = 9$ level of $\bar{p}\text{-U}$ the interaction energy is of the order of 6 keV as compared with the 44 keV first excited state of the ^{238}U nucleus. This was sufficient to induce a shift in the energy levels but the resulting hyperfine structure was negligible. For muonic ^{238}U where the interaction energy is of the order of 100 keV, the hyperfine structure has been observed experimentally by McKee for the K, L and M muonic transitions.⁴⁴

If the hadron were to make the M1 Auger transition ($\Delta n = 0, \Delta \ell = 0, \Delta j = 1$) from the upper to the lower state in a fine-structure doublet, the statistical population of the fine-structure levels would be destroyed and one would not get the correct sign for the magnetic moment. Auger transitions obey the same selection rules as electromagnetic radiation, except that $\Delta \ell = 0$ transitions are not absolutely forbidden.⁴⁵ Thus, the Auger transitions of $\Delta \ell = 1$ would not affect the statistical population of the atomic levels, and Eq. (4a) is not invalidated by the occurrence of such transitions. It was thus desirable to calculate the M1 Auger rate to see if it was much less than the electromagnetic rates. Following the discussion by Burbidge and de Borde⁴⁶ the Auger rate was calculated in a nonrelativistic approximation. The largest amount of energy available is the fine-structure splitting of the \bar{p} ($n = 11$)

state in U (2.97 keV) which is sufficient to remove an electron from states of $n = 4$ or above. Hydrogenic wave functions were employed both for the antiproton and the atomic electrons, the latter being assumed to be in the $4s$ state since s states have the greatest wave function overlap with the \bar{p} at low n . Screening of the $4s$ electron due to inner electrons and the \bar{p} was taken into account by using an effective Z for the electron as described by Slater.⁴⁷ The antiproton was assumed to be in an $n = 11, \ell = 10$ state. The number of transitions per second is given by⁴⁸

$$P_A = \left| \frac{1}{\hbar} \iint \chi_F^* \psi_F^* \frac{e^2}{r_{12}} \chi_i \psi_i d\tau_1 d\tau_2 \right|^2$$

where $\chi_{i,F}$ are the initial and final \bar{p} wave functions, and $\psi_{i,F}$ are the initial and final electron wave functions respectively. The results of this calculation yielded $P_A = 9 \times 10^7 \text{ sec}^{-1}$ which is much less than the radiative rate $P_R = 9.6 \times 10^{16} \text{ sec}^{-1}$.

III. EXPERIMENTAL PROCEDURE AND DETAILS

A. Introduction

The data were taken using a secondary beam produced by the slow extracted proton beam of the Brookhaven National Laboratory alternating gradient synchrotron (AGS). Secondary particles (π^- , K^- , \bar{p}) at 800 MeV/c or 750 MeV/c momentum were brought through an electrostatic separator which permitted selection of a K^- or \bar{p} beam which was then brought to focus on the experimental target. The stopping particles were detected and identified by means of a scintillation counter telescope. The anti-protons or kaons were slowed down in Cu or Fe degrader in combination with graphite or Be and were brought to rest in a high Z target. Targets of Pt, Au, Pb, and U were employed for the $K^- - \Sigma^-$ experiments while the \bar{p} were stopped in either Pb or U. The resulting hadronic x rays were observed with a lithium drifted germanium (Ge(Li)) detector whose pulse height was digitized and stored in a multichannel pulse height analysis system if a detected x ray occurred within 100 nsec of the arrival of a K^- or \bar{p} at the target.

B. Beam Description

The beam, designed by J. Fox, is described elsewhere.⁴⁹⁻⁵² The slow extracted proton beam from the AGS impinged upon a production target of either Cu or W. The resulting secondary beam particles entered

a magnetic lens system at an angle of 10.5° from the forward direction with a solid angle acceptance of 2.7 msr. The magnetic lens system, (shown schematically in Ref. 51), consisted of six quadrupole magnets and three dipoles, with the last dipole and quadrupole being movable so as to produce a momentum recombined or momentum dispersive beam at the final focus. The momentum slit was set to accept a $\pm 2\%$ momentum spread centered for the K^- beam on 800 MeV/c and on 750 MeV/c for \bar{p} . All of the \bar{p} data described here were taken using the momentum dispersive beam as were kaonic data in natural Au, Pb, and depleted U. Natural Pt, Pb and ^{208}Pb were used as targets in the K^- work done in the recombined beam. These beams were brought to focus on targets placed about 1.7 m behind the last quadrupole.

The desired particles (K^- or \bar{p}) were selected out of those produced at the production target by the electrostatic separator, with additional requirements imposed by the counter and logic arrangements described below. The K^-/π^- ratio varied between 0.10 to 0.16 depending on the mass slit opening and the π^-/\bar{p} ratio was approximately 75.

Production targets 5.08 cm and 7.62 cm in length were employed. For both the \bar{p} and K^- beams, the number of particles per beam burst could be increased by using the larger target; however, this change lessened the beam purity and increased the spot size.

Several degrader arrangements were used but all consisted of Cu or Fe followed by a low Z element such as C or Be. The low Z degrader was placed on the downstream side to minimize multiple scattering, which is predominantly a problem at low energies. With a 4 g/cm^2 thick

experimental target the stop rate was approximately $150 \bar{p}$ per 1×10^{12} protons incident on the production target and $2000 K^-$ per 1×10^{12} incident protons.

C. Counter Arrangement and Electronic Logic

Although there existed slight differences between the counters and logic used to define \bar{p} 's and K^- 's, the two were quite similar. The scintillation counter arrangement is shown in Fig. 3. Counters 1 through 5 were plastic scintillation counters and C was a Cerenkov counter. In the \bar{p} beam C was a Lucite threshold Cerenkov counter used to reject pions and was placed in anticoincidence with counters 1234. For the K^- beam, C was a Fitch-type Cerenkov counter⁵³ used to select kaons in the incident beam and was placed in coincidence with counters 1, 2, 3 and 4.

The Fitch counter consisted of a Lucite radiator viewed by six RCA 8850 photomultiplier tubes arranged symmetrically. Since the Fitch counter is a velocity selection device, Cerenkov light from an 800 MeV/c K^- escaped from the radiator while light from 800 MeV/c pions did not. By requiring two or more of the photo-tubes to register pulses coincidentally, effects due to beam particles entering the radiator at slightly different angles were cancelled.

Counter 3 was a $10.16 \times 10.16 \times 1.27$ cm counter viewed by two photomultiplier tubes which were required to give coincident signals. The outputs from the 10th dynode of each tube were added linearly and this sum was used to impose a dE/dx requirement on the stop signature. Counter 4 was a 0.16 cm thick 10.16×10.16 cm counter for the dispersive beam and 12.7×10.2 cm for the recombined beam.

Counter 5, a 30.5 x 30.5 x 0.64 cm scintillator placed 0.5 m behind the x ray target, was used as a veto counter for differential range measurements in the \bar{p} runs and early K^- runs. Since $\bar{5}$ seemed to improve the x-ray signal to noise, it was left in the stop signature for later K^- runs. The use of $\bar{5}$ did cause rejection of some true K^- or \bar{p} events due to production of prompt pions from nuclear capture. This effect was small however, since counter 5 subtended less than 5% of 4π solid angle at the target.

A time of flight requirement was placed on the stop signature for the \bar{p} runs by means of a small plastic counter, Z, placed in front of the mass slit (approximately 8 m upstream of the x-ray target). The delay between Z and 1234 was adjusted such that only particles with the transit time characteristic of a 750 MeV/c \bar{p} were accepted. The resulting stop signature for a \bar{p} was then $12\bar{C}3(dE/dx)4Z$. For K^- , the stop signature was $12C3(dE/dx)4\bar{5}$.

D. X Ray Detection

During the course of the experiment several Ge(Li) detectors were employed, but all useable data were taken with two 50 cm³ true coaxial detectors manufactured by Princeton Gamma-Tech. These exhibited resolutions of 1.10 keV and 0.98 keV full width at half maximum (FWHM) at 292 keV, the energy of the lead $K^-(9-8)$ transition. The preamplifiers were both of the cooled FET type and were furnished by the manufacturer as an integral part of the detector.

The preamplifier signal was fed into a linear amplifier (Ortec 452 or Princeton Gamma-Tech 340) the output of which went directly to the

analog to digital converter (ADC) of a 4096 channel multichannel analyzer (Kicksort 711A) equipped with a two-point digital stabilizer. All data were accumulated using this system or a similar one, both of which were interfaced such that the contents of memory could be written on magnetic tape.

The energy response of the detector-analyzer system was obtained using radioactive sources. In estimating yields it was necessary to know the energy efficiency of the detector system. The efficiency, Eff, can be defined by

$$\text{Eff} = N \frac{\text{RI}_{\text{obs}}}{\text{RI}}$$

where N is a normalization factor which can be chosen such that Eff is an absolute energy efficiency, RI is the relative intensity of a gamma ray, and RI_{obs} is the observed relative intensity. This efficiency was measured by placing at the target position a radioactive source containing many lines of known relative intensity and accumulating a spectrum. All electronic gating requirements except the K^- or \bar{p} stop were employed to be certain the electronic influence on the relative efficiency was also measured. The resulting spectrum was then analyzed by a least squares fitting routine which gave the area under each peak. From this the observed relative intensity was determined. The absolute efficiency was then determined by fixing one (or more) points on the curve with a source of calibrated intensity thereby determining N. The efficiency curve for the detector with 1.1 keV resolution is shown in Fig. 4. To estimate yields, corrections for self-absorption of x rays in the target were applied in addition to the detector efficiency correction.

The instrumental line shape should generally be Gaussian assuming high charge collection efficiency in the Ge(Li) detector. If neutron damage occurs in the Ge crystal caused by fast neutrons present in the experimental area, a low energy tail will develop on the peaks in the spectrum because of charge trapping in lattice defects created by the neutrons. Only for K^- data taken with the momentum recombined beam was this effect significant. In this case the instrumental shape could be well determined using the unbroadened K^- lines and calibration lines from radioactive sources.

E. Fast-Slow Timing

Due to the difference in pulse durations from fast plastic scintillators (nanoseconds) and Ge(Li) detectors (microseconds) it was necessary to form a so-called "fast-slow coincidence" at some point in the electronic logic in order to insure that x rays were in time coincidence with the corresponding stopped beam particle. The electronic logic used is shown in Fig. 5. One of the preamplifier outputs was sent through the first stages of an amplifier (Tennelec TC 200) and then to a timing discriminator (Canberra extrapolated zero strobe). The output of the timing discriminator was put in coincidence with a stop signal from the fast logic, the γ signal input being a few nanoseconds wide and the stop signal 60 to 120 ns in width. This latter width was determined from the output spectrum of the time to amplitude converter shown in Fig. 5. The delay between the stop and γ signals was adjusted such that the output of the γ -stop coincidence used to gate a multichannel analyzer

permitted storage of only that part of the timing spectrum corresponding to the prompt peak. Since the time interval of the region stored depended on the width of the stop pulse, its width was adjusted so the entire prompt peak was stored in the analyzer memory. Once the correct width and delay were obtained, the output of the γ -stop coincidence was used to gate the multichannel analyzer for the energy signal from the Ge(Li) detector.

F. Energy Calibration and Stabilization

In order to determine the energies of the observed hadronic x rays, it was necessary to calibrate the detector-analyzer system with radioactive sources whose γ -ray energies were in the energy range of interest. Due to count rate dependence of the response of the system, it was imperative to calibrate under conditions as close as possible to those under which the data were taken. This was accomplished by placing sources near the detector and increasing the width of the stop pulse to 6 μ sec. This permitted any γ within this period following a stopped beam particle to be stored in the analyzer memory. This method of calibration also had the advantage of simultaneously accumulating calibration lines and x-ray lines in the same spectrum. The longer stop pulse width resulted in a degraded hadronic x-ray signal-to-noise ratio by a factor of three. During all data and calibration runs two γ -ray sources (^{145}Ce at 145.43 keV and ^{137}Cs at 661.635 keV) were placed near the detector. A two-point digital stabilizer continuously monitored and corrected the gain and intercept of the ADC to insure that these two energies were kept

centered in preselected channels in the analyzer. The system was stabilized during the beam off portion of the AGS pulse cycle by the following method. A "beam off" gate was generated and used to inhibit the memory "add-1" command of the multichannel analyzer. Any γ ray which was detected during this beam off time was digitized but not added to memory. This digitization permitted the stabilizer to correct changes in gain, but prevented source lines from accumulating in the data. During the beam spill, only γ -ray events in coincidence with stopped beam particles were digitized, and these were added to memory. The stabilization sources were placed sufficiently far from the detector to ensure a low counting rate and almost no accidental coincidences between stabilization γ rays and stopped beam particles occurred. During the calibration runs the stabilization lines came in sufficiently slowly that corrections during any single beam spill were negligible. This method of stabilization is valid so long as the beam rate is kept reasonably steady, as it was during the course of the experiment.

The above calibration procedure was not used for the \bar{p} data taken in our earlier runs. A slightly different scheme was employed whereby during calibration runs the system was allowed to stabilize during beam-on as well as beam-off periods, but only during beam-off times for x-ray data accumulation itself. The different stabilization methods used in calibration vs. data runs resulted in a zero shift in the calibration spectra which yielded an accurate gain calibration (eV/channel) but a less accurate absolute energy calibration due to the beam-on beam-off intercept shift. Consequently, although it was straightforward to

measure a fine-structure splitting from these data, absolute \bar{p} x-ray energies were obtained to less precision.

G. Targets

The x-ray targets used in this work were positioned in a "V" configuration with the detector positioned at the inside of the V. This configuration presented a maximum target thickness to the beam while minimizing the thickness the x rays had to traverse before escaping from the target. For the $K^- - \Sigma^-$ experiments one had to insure that the target was not so thin as to permit too large a fraction of the produced hyperons to escape. For a detailed description of the targets used see Table 1.

IV. DATA ANALYSIS

The x-ray data were analyzed using a standard least squares fitting routine.⁵⁴ The analysis was carried out on the William and Mary IBM 360/50 and the Brookhaven National Laboratory CDC 6600 computers. For all x-ray transitions analyzed in this work, the natural (Lorentzian) line width was so narrow that the experimentally observed line shape was the instrumental one imposed by the Ge(Li) detector system. This was taken to be Gaussian but was modified to include a low energy exponential tail when the response of the detector changed due to charge trapping in lattice defects caused by neutron damage. The specific functional forms used in the least squares fits are discussed below.

A. Calibration Analysis

The calibration lines from radioactive sources and K^- x rays were fitted to a Gaussian function plus an exponential background of the form

$$\begin{aligned} F(x) &= A \exp \left\{ -(x - x_0)^2 / 2\sigma^2 \right\} + B_0 \exp \left\{ \lambda(x - x_0) \right\} \\ &= \mathcal{G}(x) + B(x) \end{aligned} \tag{6}$$

where x_0 was the Gaussian center, σ the FWHM divided by 2.3546, A the amplitude of the Gaussian, B_0 the background height under the peak center, and λ was an exponential constant for the background. In those cases

where a low energy tail was present, the fitting region was divided into two parts. A parameter ξ was defined such that for $x \leq (x_0 - \xi)$ the function $\mathcal{G}(x)$ was replaced by an exponential of the form

$$T(x) = A \exp \{2\xi[x - (x_0 - \xi/2)]/2\sigma^2\} \quad x \leq (x_0 - \xi) \quad (7)$$

where the other parameters have the same meaning as in Eq. (6). The functional form was chosen such that both the functions and their derivatives were continuous at the matching point $(x_0 - \xi)$.

The replacement of the Gaussian by an exponential on the low energy side was necessary only in the last $K^- - \Sigma^-$ data accumulated. For the analysis of the $\Sigma^-(12 \rightarrow 11)$ fine-structure components, the adjacent $K^-(9 \rightarrow 8)$ was first fitted with the parameter ξ free. Although within statistics this value of ξ agreed with that obtained by fitting lines from radioactive sources, the shape used in the Σ^- analysis was taken from the adjacent $K^-(9 \rightarrow 8)$ transition because it was accumulated under conditions identical to the $\Sigma^-(12 \rightarrow 11)$ accumulation.

To obtain an absolute energy calibration of the Ge(Li)-multichannel analyzer system, the centroids of lines of known energies were used. A least squares fit was performed with first, second, and third order polynomials. The best fit was determined by using the F value⁵⁵ to test the validity of the additional term. Once the best fit representing energy as a function of channel number was determined, the energies of the hadronic x rays could be obtained.

B. Analysis for Fine-Structure Splitting

Except for the $\bar{p}(11 \rightarrow 10)$ transition in U, the two fine-structure components in a \bar{p} or Σ^- x ray were separated by less than one FWHM,

i.e., these lines did not satisfy Rayleigh's criterion for the resolution of two spectral lines.⁵⁶ It was necessary to develop a method of analysis for these data which permitted one to determine the separation of the two centroids. These two unresolved components will be referred to as a doublet in the following discussion.

The functional form for a doublet was defined as

$$D(x) = RA_2 \exp \{-(x - x_0)^2/2\sigma^2\} + A_2 \exp \{-[x-(x_0 + \delta)]^2/2\sigma^2\} \quad (8)$$

where A_2 was the amplitude of the second component, and δ the separation between centers of the two components. The widths of the two Gaussians were assumed to be equal thereby making R (= Amplitude (1)/Amplitude (2)) the ratio of areas as well as the ratio of amplitudes for the doublet members. The statistical ratio a/c as defined by Eq. (4) was used for R , and it was held fixed. Since the noncircular transitions also contributed to the observed line, a second doublet function $D'(x)$ was defined as,

$$D'(x) = R'A_2 \exp \{-(x - x'_0)^2/2\sigma^2\} + A_2 \exp \{-[x-(x'_0 + \delta')]\^2/2\sigma^2\} \quad (9)$$

where x'_0 was the different center due to the j dependence of the solution to the Dirac equation, δ' was the splitting of the noncircular doublet as given by Eqs. (3), (5), and R' was the ratio defined by Eq. (4).

The resulting functional form was

$$F(x) = D(x) + GD'(x) + B(x) \quad (10)$$

with the background term taken to be the same as in Eq. (6). The amount of noncircular contribution included, $G(= \alpha/\gamma$ in Fig. 2), was estimated

from either the experimentally determined ratio I , or from a cascade calculation, both of which are discussed in Section II. For the \bar{p} data where such an estimate of G was not possible for the transitions of lower n , G was permitted to be a free parameter in the least squares fit, provided that the fit converged. If the fit did not converge, then G was estimated from the cascade program and held fixed. Fits were then performed over a range of values of G , the range being determined by the range of predictions of the cascade program for relative yields of the higher n ($\Delta n = 2$) and ($\Delta n = 1$) transitions. It should be noted that the addition of $D'(x)$ added no more independent parameters because both x'_0 and δ' were related to x_0 and δ through the Dirac equation. In those situations where it was necessary to include an exponential tail on the low energy side, each Gaussian was treated separately using the parameter ξ , discussed above, which was determined from the $K(9 \rightarrow 8)$ transition.

In the \bar{p} transitions where the separation between the two doublet components was sufficiently large, the separation was treated as a free parameter. The ratio of areas was held fixed as described above. For the higher transitions, the width was also held fixed. The data were fit with three different widths: the measured instrumental width, the measured width plus its standard error, and the measured width minus its standard error.

If the separation between the doublet components was less than 40% of one FWHM, it became necessary to hold the separation fixed for a given fit. It was no longer valid to let δ be a free parameter because the error determined from the error matrix reached the same order of

magnitude as the value obtained for δ . One thus needed to use the range over which χ^2 changed by one unit as the standard error rather than the value obtained from the error matrix, since the criterion of requiring χ^2 to change by one unit is always valid so long as one can make a parabolic expansion of the χ^2 hypersurface in the region of the χ^2 minimum.⁵⁵ One should note that for errors much less than the parameter, the two methods give the same value for the standard error. For each fit the free parameters included the background amplitude and exponential constant, the center of the first Gaussian (the second center being a distance δ away) and the amplitude of the second Gaussian (the amplitude of the first Gaussian being determined by RA_2). All widths were assumed equal and held fixed.

A series of fits was made on each fine-structure doublet, with the separation δ fixed for each fit. By fitting over a range of δ it was possible to obtain χ^2 as a function of δ thus enabling one to obtain "most probable" values for δ . Since δ is the difference of the fine-structure splittings for successive n levels, a value for the magnetic moment was thereby obtained. For $n \geq 10$ the ratio R ($= a/c$, Eq. (4b)), differs from unity by 10% or less, and it was not always possible to obtain a clear indication of the sign of the magnetic moment.

For the $\bar{p}(12 \rightarrow 11)$ and $(11 \rightarrow 10)$ lines in both Pb and U this sign was unambiguous. Fits to the Σ^- data were sensitive to the magnitude of the magnetic moment, and there was an indication of a preference for a negative sign. The value of the magnetic moment was taken to be

the point at which the χ^2 function reached a minimum and the statistical error was taken to be the interval over which χ^2 changed by one unit.⁵⁵

The instrumental width of the lines used in the series of least squares fits was determined from the following considerations. The observed $K^-(9 \rightarrow 8)$ x ray is a superposition of two transitions: that between the energy levels $(n = 9, \ell = 8) \rightarrow (n = 8, \ell = 7)$ and that for $(9, 7) \rightarrow (8, 6)$. The Klein-Gordon energies of these two components differ by 586 eV which corresponds, for our resolution, to a difference of about 0.5 FWHM. (The amplitude ratio of circular/noncircular transitions is approximately 5.) This small noncircular contribution tends to broaden the width and shift the centroid higher in energy if the two peaks are fit to a single Gaussian. The $K(9 \rightarrow 8)$ was fit to a doublet function (see Eq. (8)) over a range of R , the relative separation set equal to that predicted by the Klein-Gordon equation, and all other parameters free. The effect of R on the width is displayed in Fig. 6. The cascade program predicted $R = 5.2$ which corresponds to a width of 7.57 channels. An error of 15% was assigned to the ratio, R , obtained by this method because the cascade program predicted the relative yields of the kaonic x rays to better than 15%. This uncertainty in R corresponded to a range of width in channels from 7.50 to 7.65, and agreed with that predicted from calibration lines, (7.4 ± 0.3) . The $K(9 \rightarrow 8)$ transition at 292 keV when fit to a single Gaussian exhibited the same width in the calibration run as it did in the data runs (8.2 ± 0.3) , a width considerably broader than the γ -ray lines at 276 keV (7.02 ± 0.29) and 303 keV (7.71 ± 0.15) from ^{133}Ba . This served to confirm the conclusion that the broadening

in the $K(9 \rightarrow 8)$ line was due to the first noncircular transition and not, for example, from pileup in the detector during the beam spill. Thus one could use a considerably narrower instrumental width than the single Gaussian fit to the $K(9 \rightarrow 8)$ would indicate. The instrumental width was taken to be the central value in the range determined from the cascade program, and the error taken to be the quadrature of the errors due to the uncertainty in R and that due to statistical uncertainty from the least squares fit with R equal to its central value.

For the \bar{p} data, the width calibration was taken from K^- x rays accumulated for an Au target under the same conditions as the \bar{p} data were taken, and from calibration runs.

Since the instrumental width was held fixed in generating the χ^2 function vs. doublet separation δ , it was necessary to vary the width over the range of its experimental uncertainty and to study its effect on the magnetic moment. The values derived from the data reflect both the uncertainty in instrumental width and in G , the contribution from the noncircular transitions.

C. Data Simulation

In order to test the least squares fitting routines used and to study the effect of contributions from inner transitions when they were well known, simulated data were generated with a computer. The input to the program was the functional form given by Eq. (10), which was then randomized with Gaussian statistics. These simulated data were then analyzed by the same least squares fitting routine used to fit the actual

data. The results of analysis of the simulated data exhibited the same sensitivity to G as did those obtained from experimental data and added to the confidence with which one could view the results.

V. RESULTS AND CONCLUSIONS

For a determination of the magnetic moment one needs to know the particle's mass in order to compute the reduced mass used in Eq. (3). Although the tabulated masses, $m_p = (938.2592 \pm 0.0052)$ MeV, and $m_{\Sigma^-} = (1197.34 \pm 0.07)$ MeV were used,⁵⁷ it was possible to determine \bar{p} and Σ^- masses directly from this experiment to the degree of precision needed for the determination of the respective moments.

The errors in the values of the magnetic moments associated with the uncertainties in the contributions of noncircular transitions and in the instrumental linewidth were common to the analysis of both \bar{p} and Σ^- data. We shall discuss effects relevant to both analyses before presenting the values obtained.

A. Noncircular Transitions

Simulated data were generated using values of G (see Eq. (10)) ranging from 0.0 to 0.25 with the width, total number of counts and background being taken from the set of $K^- - \Sigma^-$ data in Pb with the greatest number of K^- stops. For each set of simulated data, the computer random number generator was reset to the same initial value to insure that the only variable among the different sets of data was the value of G .

The results of this analysis of the simulated data showed that the value obtained for the magnetic moment is very sensitive to the contribution for the first noncircular transition. Similarly, simulated

data were generated for several \bar{p} transitions and the analysis showed the magnetic moment to be extremely sensitive to the contributions from the first noncircular transition. This was also found to be the case if G was varied in the Σ^- or \bar{p} analysis.

G was fit as a free parameter in the analysis of the $U-\bar{p}$ ($12 \rightarrow 11$) and \bar{p} ($11 \rightarrow 10$) transitions and in the $Pb-\bar{p}$ ($11 \rightarrow 10$) transition. For the higher transitions G was determined from the data, if the appropriate $\Delta n = 2$ transition was in the experimentally obtained spectrum, or from a cascade calculation if it was not.

The set of $K^- - \Sigma^-$ data representing the largest number of K^- stops was analyzed for the Σ^- ($12 \rightarrow 11$) fine structure splitting for two extreme values of G . These values were chosen from both the Σ^- and \bar{p} data from the following considerations. Since the Σ^- atomic energy levels in Pb have approximately the same Bohr radii as the corresponding \bar{p} levels in U , we chose a range of G which was consistent with the $U-\bar{p}$ ($12 \rightarrow 11$) analysis and with the upper limit obtained directly from the Σ^- data. We thus chose a range of 0.05 to 0.15 for G in the $Pb \Sigma^-$ analysis. The results of the analysis for $G = 0.05$ and $G = 0.15$ for these data are shown in Fig. 7. The region over which χ^2 changed by one unit was approximately the same for the two values of G , but the center was shifted. The region size was increased by 20% if one took the upper limit from the $G = 0.15 \chi^2$ curve and the lower limit from the $G = 0.05$ one. Similarly, the region for G was chosen to be from 0.10 to 0.20 for Pt .

B. Instrumental Width Uncertainties

When a single Gaussian such as a computer-simulated line or a radioactive source line in a calibration run was fit with a doublet

function with $R = 1.096$ (the value from Eq. (4b) for a circular $(12 \rightarrow 11)$ transition) and a fixed instrumental width, the χ^2 function was centered about zero separation, but there was a finite interval over which χ^2 changed by one unit. This range was a reflection of statistical uncertainties in the width of the single Gaussian. Simulated data were generated with single Gaussians of differing amplitudes on the same background. As the amplitude was increased, the region over which χ^2 changed by one unit decreased as one would expect, because a single Gaussian fit to each one showed that with better signal-to-background, uncertainties in the extracted width decreased.

Since the instrumental widths each had an associated statistical error, it was necessary to carry out the doublet analysis on the \bar{p} or Σ^- data for several widths and to include the effects of their uncertainties in the quoted errors. For sufficiently large separations between the doublet components such as were present for the $Pb-\bar{p}$ ($12 \rightarrow 11$) and ($11 \rightarrow 10$) and the $U-\bar{p}$ ($13 \rightarrow 12$), ($12 \rightarrow 11$) and ($11 \rightarrow 10$) transitions, there was little sensitivity to the width used, and in fact, a change of five standard deviations in the instrumental width for the last two lines in U caused less than a 2% change in the extracted value of $\mu(\bar{p})$.

C. Statistical Population of Fine-Structure Levels

The fine-structure components of the \bar{p} ($11 \rightarrow 10$) in U were separated by more than one FWHM so it was possible to make a free fit to all parameters including G of a doublet function plus an exponential background. The only constraint was that the two component lines have the same width. This fit provided a measurement of the ratio R (Eq. (8)).

The result was $R = 1.27 \pm 0.19$ which was in agreement with 1.11, the value obtained using Eq. (4b). One can thus conclude that the statistical population of the fine-structure states is not significantly changed by, e.g. M1 Auger transitions, a result which agrees with the calculation discussed in section II. The assumption that R (and R') could be held fixed and equal to the values obtained from Eq. (4a) appears reasonable.

D. Dependence of Results on Region of Fit

The spectra obtained from \bar{p} in Pb and U, and K^- in Pt and ^{208}Pb are displayed in Figs. 8 through 11. In the \bar{p} data the lines were well separated and there was no problem choosing a region over which to fit a given transition, i.e. an ample region of background could be included on both sides of the relevant peak. Due to the close proximity of the K^- ($9 \rightarrow 8$) and K^- ($14 \rightarrow 11$) on the high and low energy sides respectively of the Σ^- ($12 \rightarrow 11$), the dependence of the χ^2 function on the region over which the data were fit was studied. Fig. 12 shows a series of χ^2 functions generated by successively decreasing the region of fit by one channel on each side of the Σ^- ($12 \rightarrow 11$) in ^{208}Pb (with $G = 0$). Although there were slight fluctuations in the χ^2 function, it was not statistically significant. The other Σ^- data exhibited a similar independence of the region over which the fit was made.

E. The Antiproton Magnetic Moment

The $\Delta n = 1$ \bar{p} transitions from the levels $n = 15$ to $n = 10$ in both Pb and U were analyzed for fine-structure splitting. The χ^2 function

obtained for the \bar{p} ($11 \rightarrow 10$) transition in U is shown in Fig. 13. One can observe that the sign of $\mu(\bar{p})$ is negative and that the two curves representing different instrumental widths almost coincide in the region of the minimum χ^2 . The results of a free fit to the U- \bar{p} ($11 \rightarrow 10$) transition are shown in Fig. 14. Table 2 is a compilation of the values obtained for $\mu(\bar{p})$ from analysis of the $\Delta n = 1$ transitions from $n = 13$ to $n = 10$ in both U and Pb.

One should note that the value for $\mu(\bar{p})$ derived from the Pb- \bar{p} ($11 \rightarrow 10$) transition, as listed in Table 2, is substantially different from the corresponding value reported previously.³⁰ This discrepancy arises from a failure to include the contribution from the first noncircular transition in the earlier analysis of the data. Transitions higher than the ($13 \rightarrow 12$) were omitted because of the large statistical uncertainty resulting from the comparatively small fine-structure splittings.

The weighted average of the values of $\mu(\bar{p})$ is

$$\mu(\bar{p}) = (-2.819 \pm 0.056) \mu_N$$

where μ_N is the nuclear magneton, $\mu_N = e\hbar/2m_p c$. The quoted error is the root-mean-square error since the six measurements of Table 2 represent a consistent set. This value is in good agreement with that of $2.793 \mu_N$ for the proton and is opposite in sign. It is also in agreement with, but much more precise than, the earlier measurement of Button and Maglic,⁵⁸ who obtained $(-1.8 \pm 1.2) \mu_N$ from a double scattering experiment in a hydrogen bubble chamber. A free fit to all parameters including G and R for the \bar{p} ($11 \rightarrow 10$) in U gave a value of $\mu(\bar{p}) = (-2.86 \pm 0.08) \mu_N$.

F. The Σ^- Magnetic Moment

Each set of Σ^- data were analyzed for fine-structure splitting and the individual curves of χ^2 vs. Σ^- magnetic moment were added together to yield the result shown in Fig. 15. The χ^2 response for the total data represented in this figure was obtained with G fixed at 0.10 for the Pb data and at 0.15 for the Pt data. The region of $\mu(\Sigma^-)$ shown between the two vertical lines in this figure represents the error due to the instrumental width but not that due to the uncertainties in the contributions from noncircular transitions. This error was increased by 20% to include uncertainties due to contributions from the noncircular Σ^- ($12 \rightarrow 11$) transition.

From Fig. 15 one notes an indication of a preference for a negative sign for the Σ^- magnetic moment, the χ^2 difference between the two minima being 0.95 for one χ^2 curve and 0.82 for the other. The final value obtained for $\mu(\Sigma^-)$ is:

$$\mu(\Sigma^-) = (-1.89 \pm 0.47) \mu_{\Sigma}$$

or equivalently

$$\mu(\Sigma^-) = (-1.48 \pm 0.37) \mu_N$$

The value for $\mu(\Sigma^-)$ differs by 1.6 standard deviations from the SU(3) value of $-0.9 \mu_N$. One should note, however, that our result is in agreement with the recent measurement of $\mu(\Xi^-)$ by Cool, et al.⁵⁹ who obtained

$$\mu(\Xi^-) = (-2.2 \pm 0.8) \mu_N .$$

Since the mass of the Σ^- is 27% greater than that of the proton, the presence of an appreciable mass correction term in the magnetic moment would not be surprising. However, as mentioned by Cool, et al.,⁵⁹ there is at present no fully acceptable method for calculating such a correction. Certainly at the present level of experimental precision no definitive disagreement with the value predicted by Eq. (2) is implied by our result.

VI. TABLES

Table 1. Target Dimensions. The thickness given is the total actual thickness of the target. In cases where several sheets of different sizes were used simultaneously, all are listed. D stands for the momentum dispersive beam and R the momentum recombined one.

| Beam | Target Material | Length (cm) | Width (cm) | Thickness (gm/cm ²) |
|------------------|-------------------|----------------|---------------|------------------------------------|
| K ⁻ D | ¹⁹⁷ Au | 9.65 | 9.65 | 8.3 |
| \bar{p} D | Natural Pb | 12.7 | 12.7 | 5.4 |
| \bar{p} D | Depleted U | 10.2 | 12.7 | 4.5 |
| K ⁻ D | Natural Pb | 12.7 | 12.7 | 6.8 |
| K ⁻ D | Depleted U | 11.1 | 14.0 | 1.55 |
| | | 10.2 | 14.0 | 1.53 |
| | | 8.6 | 11.4 | 3.03 |
| K ⁻ R | Natural Pb | 12.7 | 10.2 | 10.2 |
| K ⁻ R | Natural Pb | 12.7 | 10.2 | 6.8 |
| K ⁻ R | ²⁰⁸ Pb | 7.6 | 7.6 | 7.2 |
| K ⁻ R | Natural Pt | 12.7 | 10.2 | 6.8 |

Table 2. Magnetic moment derived from antiprotonic x rays in Pb and U. For all transitions shown, R was given by the appropriate statistical ratio a/c given by Eq. (4b). The contribution, G, of the first noncircular transition was fit as a free parameter in the data analysis for the 12 → 11 and 11 → 10 transitions in U and for the 11 → 10 transition in Pb.

| Element | Transition | $\mu(e\hbar/2m_p c)$ |
|---------|------------|----------------------|
| Pb | 13 → 12 | -2.70 ± 0.85 |
| | 12 → 11 | -2.76 ± 0.55 |
| | 11 → 10 | -2.58 ± 0.21 |
| U | 13 → 12 | -2.78 ± 0.65 |
| | 12 → 11 | -2.81 ± 0.13 |
| | 11 → 10 | -2.847 ± 0.066 |

VII. ACKNOWLEDGMENTS

The author wishes to express his appreciation to the following people for their contributions to and assistance in this work.

Dr. Robert E. Welsh, his advisor, for suggesting this experiment, for his continued interest and assistance in all phases of this research and in the preparation of this manuscript.

Dr. M. Eckhause, his advisor, for his interest and assistance in all phases of this research and in the preparation of this manuscript.

Dr. J. R. Kane for his assistance and advice in the experimental runs and for reading the manuscript.

Dr. C. R. Cox for his assistance in the experimental runs and in analysis of the data.

Dr. H. C. von Baeyer for many helpful discussions and for reading the manuscript.

Dr. R. G. Winter for helpful discussions and for reading the manuscript.

Dr. K. G. Shaver for reading the manuscript.

Dr. C. E. Carlson for helpful discussions on SU(3) symmetry and on the Auger calculation.

Dr. J. B. Delos for helpful discussions on the Auger calculation.

Dr. R. J. Powers for assistance in the experimental runs, for helpful discussions on dynamic E2 mixing and for calculating dynamic E2 shifts in U for \bar{p} , Σ^- and K^- .

Mr. J. P. Miller for his untiring assistance in preparing for and tearing down after the experimental runs as well as his invaluable assistance in taking the data and its analysis.

His other collaborators, Drs. P. D. Barnes, R. A. Eisenstein, J. D. Fox, D. A. Jenkins, A. R. Kunselman, W. C. Lam, and R. B. Sutton, for their assistance in the experimental runs as well as helpful discussions on many aspects of this work.

Dr. R. T. Siegel for informative discussions on SU(3).

Mr. W. F. Vulcan for his untiring work on the multichannel analyzer system and other electronic problems and for assistance in preparing for experimental runs.

Mr. S. G. Hummel and the staff of the William and Mary machine shop for construction of the scintillation counters and other equipment.

Dr. R. W. Southworth and the staff of the William and Mary Computer Center for their help.

Dr. F. R. Kane and Dr. G. H. Miller for their assistance and advice on data analysis and computer programming.

His fellow graduate students, M. E. Vislay, R. H. Hart and G. W. Dodson for their assistance in preparation of the experiments.

Ms. P. Hand for her untiring efforts in all aspects of the data analysis.

Mr. G. G. Evans and Mr. R. Hamilton for their assistance in the data analysis.

Mrs. Sylvia Stout for her expert typing of the manuscript.

His parents for their continued support, both financial and otherwise, during his graduate study.

His wife Julie, for her constant support and encouragement, her patience and understanding through long absences during the experimental runs, and for typing parts of the earlier drafts.

Financial support contributed by the National Science Foundation, N.A.S.A., The John Stewart Bryan Scholarship Fund and the W. A. R. Goodwin Memorial Fund.

This work was supported in part by the National Science Foundation and the U. S. Atomic Energy Commission.

VIII. REFERENCES

1. E. Fermi, E. Teller and V. Weisskopf, Phys. Rev. 71, 314 (1947).
2. E. Fermi and E. Teller, Phys. Rev. 72, 399 (1947).
3. J. A. Wheeler, Rev. Mod. Phys. 21, 133 (1949).
4. M. Conversi, E. Pancini, and O. Piccioni, Phys. Rev. 71, 209 (1947).
5. M. Camac, A. D. McGuire, J. B. Platt, and H. J. Schulte, Phys. Rev. 88, 134 (1952).
6. V. L. Fitch and J. Rainwater, Phys. Rev. 92, 789 (1953).
7. M. Y. Au-Yang and M. L. Cohen, Phys. Rev. 174, 468 (1968).
8. S. S. Gerstein, V. I. Petrukhin, L. I. Ponomarev, and Y. D. Prokoshkin, Usp. Fiz. Nauk. 97, 3 (1969) (Soviet Phys. - Uspekhi 12, 1 (1969)).
9. A. H. de Borde, Proc. Phys. Soc. (London) A 67, 57 (1954).
10. D. Zieminska, Phys. Lett. 37B, 403 (1971).
11. C. E. Wiegand, Phys. Rev. Lett. 22, 1235 (1969).
12. G. Backenstoss, T. Bunaciu, S. Charalambus, J. Egger, H. Koch, A. Bamberger, U. Lynen, H. G. Ritter, and H. Schmitt, Phys. Lett. 33B, 230 (1970).
13. W. C. Lam, P. D. Barnes, R. A. Eisenstein, J. Miller, R. B. Sutton, D. A. Jenkins, M. Eckhause, J. R. Kane, B. L. Roberts, R. E. Welsh, A. R. Kunselman, and J. D. Fox, Bull. Am. Phys. Soc. 18, 595 (1973).
14. T. E. O. Ericson, CERN Report TH.1422-CERN (1971) and Proc. of the IVth International Conference on High Energy Physics and Nuclear Structure, Dubna (1971), p. 267.

15. G. Backenstoss, Proc. of the IVth International Conference on High Energy Physics and Nuclear Structure, Dubna (1971), p. 283, and Rev. of Nucl. Sci. 20, 467 (1970).
16. C. S. Wu, Proc. of the Third International Conference on Atomic Physics, Boulder (1972), p. 93.
17. C. S. Wu, Proc. of IVth International Conference on High Energy Physics and Nuclear Structure, Dubna (1971), p. 349.
18. C. S. Wu and L. Wilets, Ann. Rev. Nucl. Sci. 19, 527 (1969).
19. S. Devons and I. Duerdoth, Adv. in Nucl. Phys. 2, 295 (1969).
20. D. West, Repts. Prog. Phys. 21, 271 (1958).
21. See, for example, W. B. Shuler, Thesis, College of William and Mary, Williamsburg, Va. (1968) and R. J. Harris, Jr., W. B. Shuler, M. Eckhause, R. T. Siegel, and R. E. Welsh, Phys. Rev. Lett. 20, 505 (1968) and P. Martin, G. H. Miller, R. E. Welsh, D. A. Jenkins, R. J. Powers, and A. R. Kunselman, Phys. Rev. C 8, 2453 (1973).
22. W. M. Bugg, G. T. Condo, E. L. Hart, H. O. Cohn, and R. D. McCulloch, Phys. Rev. Lett. 31, 475 (1973).
23. See, for example, W. W. Sapp, Jr., M. Eckhause, G. H. Miller, and R. E. Welsh, Phys. Rev. C 5, 690 (1972) for π^- widths and yields. For a discussion of nuclear correlations see the review article: D. S. Koltun, Adv. in Nucl. Phys. 3, 71 (1969).
24. See, for example, G. Backenstoss, A. Bamberger, I. Bergström, P. Bounin, T. Bunaciu, J. Egger, S. Hultberg, H. Koch, M. Krell, A. Lynen, H. G. Ritter, A. Schwitter, and R. Stearns, Phys. Lett. 38B, 181 (1972).

25. P. D. Barnes, S. Dytman, R. A. Eisenstein, W. C. Lam, J. Miller, R. B. Sutton, D. A. Jenkins, R. J. Powers, M. Eckhause, J. R. Kane, B. L. Roberts, R. E. Welsh, A. R. Kunselman, R. P. Redwine, and R. E. Segel, Phys. Rev. Lett. 29, 1132 (1972), and G. Backenstoss, A. Bamberger, T. Bunaciu, J. Egger, H. Koch, U. Lynen, H. G. Ritter, H. A. Schmitt, and A. Schwitter, Phys. Lett. 41B, 552 (1972).
26. J. Lathrop, R. Lundy, V. L. Telegdi, R. Winston, D. D. Yovanovich, and A. J. Breaden, Nuovo Cimento 17, 109, 114 (1970) and S. Devons, G. Gidal, L. M. Lederman, and G. Shapiro, Phys. Rev. Lett. 5, 330 (1960).
27. G. Backenstoss, T. Bunaciu, S. Charalambus, J. Egger, H. Koch, A. Bamberger, U. Lynen, H. G. Ritter, and H. Schmitt, Phys. Lett. 33B, 230 (1970).
28. J. Dugan, Y. Asano, M. Y. Chen, S. C. Cheng, E. Hu, L. Lidofsky, W. Patton, C. S. Wu, D. Lu, and V. Hughes, Bull. Am. Phys. Soc. 19, 599 (1974).
29. A. Bamberger, U. Lynen, H. Piekartz, J. Piekartz, B. Povh, H. G. Ritter, G. Backenstoss, T. Bunaciu, J. Egger, W. D. Hamilton, and H. Koch, Phys. Lett. 33B, 233 (1970).
30. J. D. Fox, P. D. Barnes, R. A. Eisenstein, W. C. Lam, J. Miller, R. B. Sutton, D. A. Jenkins, R. J. Powers, M. Eckhause, J. R. Kane, B. L. Roberts, M. E. Vislay, R. E. Welsh, and A. R. Kunselman, Phys. Rev. Lett. 29, 193 (1972).
31. J. D. Fox, W. C. Lam, P. D. Barnes, R. A. Eisenstein, J. Miller, R. B. Sutton, D. A. Jenkins, M. Eckhause, J. R. Kane, B. L. Roberts, R. E. Welsh, and A. R. Kunselman, Phys. Rev. Lett. 31, 1084 (1973).

32. See, for example, J. J. Sakurai, Invariance Principles and Elementary Particles, (Princeton Univ. Press., Princeton, New Jersey, 1964) p. 148.
33. See, for example, J. Bernstein, G. Feinberg, and T. D. Lee, Phys. Rev. 139, B1650 (1965).
34. M. Nauenberg, Phys. Rev. 135, B1047 (1964).
35. S. Coleman and S. L. Glashow, Phys. Rev. Lett. 6, 423 (1961).
36. H. R. Rubinstein, F. Scheck, and R. H. Solocow, Phys. Rev. 154, 1608 (1967).
37. For a discussion of magnetic moments and fine structure splitting see: H. A. Bethe and E. Salpeter, Quantum Mechanics of One- and Two - Electron Atoms (Academic, New York, 1957), starting with sect. 10, also J. J. Sakurai, Advanced Quantum Mechanics, (Addison-Wesley, Reading, Mass., 1967) sect. 3-5.
38. W. W. Sapp, Jr., College of William and Mary Report, WM70-21 (1970) and Ref. 23.
39. L. Wilets, Kgl. Danske Videnskab. Selskab, Mat. - Fys. Medd. 29, 3 (1954).
40. B. A. Jacobsohn, Phys. Rev. 96, 1637 (1954).
41. M. Y. Chen, Phys. Rev. C 1, 1176 (1970).
42. G. Ara and M. Y. Chen, Bull. Am. Phys. Soc. 19, 599 (1974).
Similar results have been obtained by R. J. Powers (private communication).
43. S. C. Cheng, Y. Asano, M. Y. Chen, J. Dugan, E. Hu, L. Lidofsky, W. Patton, C. S. Wu, D. Lu, and V. Hughes, Bull. Am. Phys. Soc. 19, 599 (1974).

44. R. J. McKee, Phys. Rev. 180, 1139 (1969).
45. Y. Eisenberg and D. Kessler, Nuovo Cimento 19, 1195 (1961).
46. G. R. Burbidge and A. H. de Borde, Phys. Rev. 89, 189 (1953).
47. J. C. Slater, Quantum Theory of Atomic Structure, Vol. I (McGraw-Hill, New York, 1960) p. 368 ff.
48. P. A. M. Dirac, Proc. Roy. Soc. (London) A114, 243 (1927).
49. J. D. Fox, BNL Accelerator Dept. EP & S Division Technical Note No. 7 (1967).
50. J. D. Fox, BNL Accelerator Dept. EP & S Division Technical Note No. 20 (1968).
51. M. Zeller, L. Rosenson, and R. E. Lanou, Jr., BNL AGS Summer Study, BNLL16000 (1970).
52. A. S. Carroll, T. F. Kycia, K. K. Li, D. N. Michael, P. M. Mockett, D. C. Rahm, and R. Rubinstein, BNL Accelerator Dept. EP & S Division Technical Note No. 54 (1972).
53. V. Fitch and R. Motley, Phys. Rev. 101, 496 (1956). For a discussion of Cerenkov counters see B. J. Moyer in Nuclear Instruments and Their Uses, W. Shell, ed. (John Wiley, New York 1962) p. 166.
54. For a description of the method of least squares fitting used here see R. H. Moore and R. K. Ziegler, Los Alamos Report LA-2367 (1960).
55. See, for example, P. R. Bevington, Data Reduction and Error Analysis for the Physical Sciences (McGraw-Hill, New York, 1969).
56. See A. Sommerfeld, Optics (Academic Press, New York, 1964) p. 289.
57. Particle Data Group, Rev. Mod. Phys. 45, S16 (1973).
58. J. Button and B. Maglic, Phys. Rev. 127, 1297 (1962).
59. R. L. Cool, G. Giacomelli, E. W. Jenkins, T. F. Kycia, B. A. Leontic, K. K. Li, and J. Teiger, Phys. Rev. Lett. 29, 1630 (1972).

IX. FIGURE CAPTIONS

- Fig. 1 EL transitions between two fine-structure states.
- Fig. 2 Schematic diagram of circular and non-circular transitions considered in the analysis of the Σ x-ray data. Levels are labeled by (n, ℓ) values. The fine structure splittings are not shown.
- Fig. 3 Target and counter geometry drawn to approximate scale. The Pb shielding was 0.6 m thick in the direction of the beam. Counter 4 was placed immediately upstream of the target.
- Fig. 4 Absolute energy efficiency of the Ge(Li) detector which exhibited 1.10 keV resolution at 292 keV. The efficiency of the second detector was almost identical. This figure excludes solid angle factors.
- Fig. 5 Fast-slow and gating logic used with the multichannel analyzer. The output of BO was the "beam off" signal and that of S the particle stop signature. PA was the cooled FET preamplifier, A1 and A2 linear amplifiers (see text), TD the timing discriminator, and TAC was the time to amplitude converter.
- Fig. 6 Instrumental resolution extracted as a function of the ratio of the circular to first non-circular transitions for the $K^-(9 \rightarrow 8)$ transition in Pb. The FWHM is given in channels with one channel corresponding to 148 eV. The dashed line represents the width obtained from a single Gaussian fit to the complex $K^-(9 \rightarrow 8)$ line.

Fig. 7 χ^2 -response from fitting $\Sigma^-(12 \rightarrow 11)$ in natural Pb with 2 different values of G (Eq. (10)). The region between the dashed vertical bars is the range over which χ^2 changes by 1 unit for the curve with $G = 0.05$. The region between the solid vertical bars is the range over which χ^2 changes by 1 unit for the curve with $G = 0.15$.

Fig. 8 X-ray spectrum obtained by stopping \bar{p} in natural Pb. The data represent $4.5 \times 10^8 \bar{p}$ stops.

Fig. 9 X-ray spectrum obtained by stopping \bar{p} in U. The data represent $4.9 \times 10^6 \bar{p}$ stops.

Fig. 10 X-ray spectrum obtained by stopping K^- in Pt. The data represent $3.6 \times 10^8 K^-$ stops.

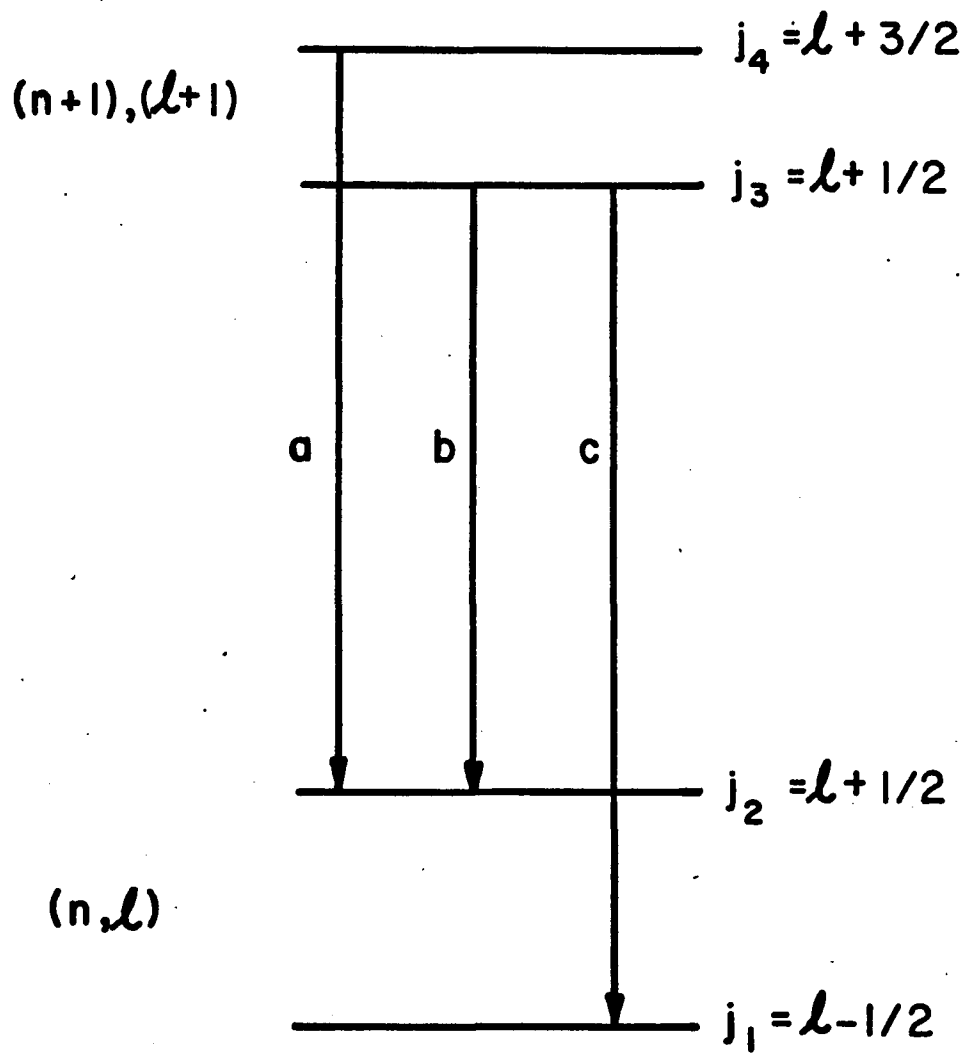
Fig. 11 X-ray spectrum obtained by stopping K^- in ^{208}Pb . The data represent $8.3 \times 10^7 K^-$ stops.

Fig. 12 χ^2 response generated for several regions of fit for the $\Sigma^-(12 \rightarrow 11)$ transition in ^{208}Pb with $G = 0$. Each successive curve was generated by decreasing the region by one channel on each side. The number of degrees of freedom is indicated by ν .

Fig. 13 χ^2 response for the $\bar{p}(11 \rightarrow 10)$ transition in U. The χ^2 difference between the two minima is 6.7. The two curves plotted are for instrumental widths that are one standard deviation greater and one standard deviation less than the measured value.

Fig. 14 $\bar{p}(11 \rightarrow 10)$ transition in U. The smooth curve represents a free fit to the data.

Fig. 15 χ^2 response from fitting the Σ^- ($12 \rightarrow 11$) transitions. The curves represent a compilation of data from natural Pb (5.4×10^8 K^- stops), ^{208}Pb (8.3×10^7 K^- stops), and Pt (3.6×10^8 K^- stops). The solid curve was calculated for instrumental resolution that was one standard deviation greater than the most probable; the dotted curve for one standard deviation less. Included in the error for the Σ^- moment (see text) but not indicated in this Fig. is the uncertainty introduced by contributions from non-circular transitions.



- FIG. 1

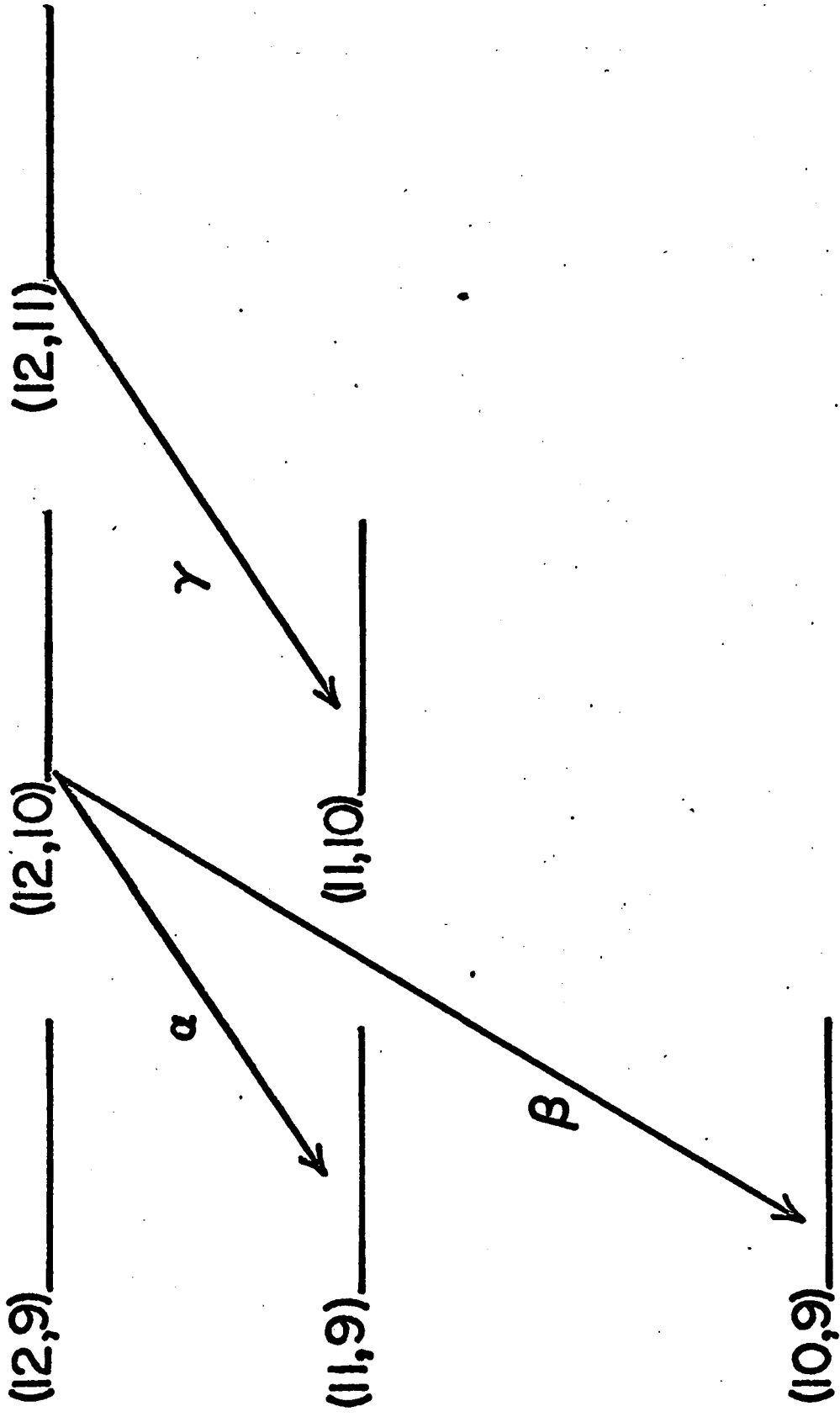
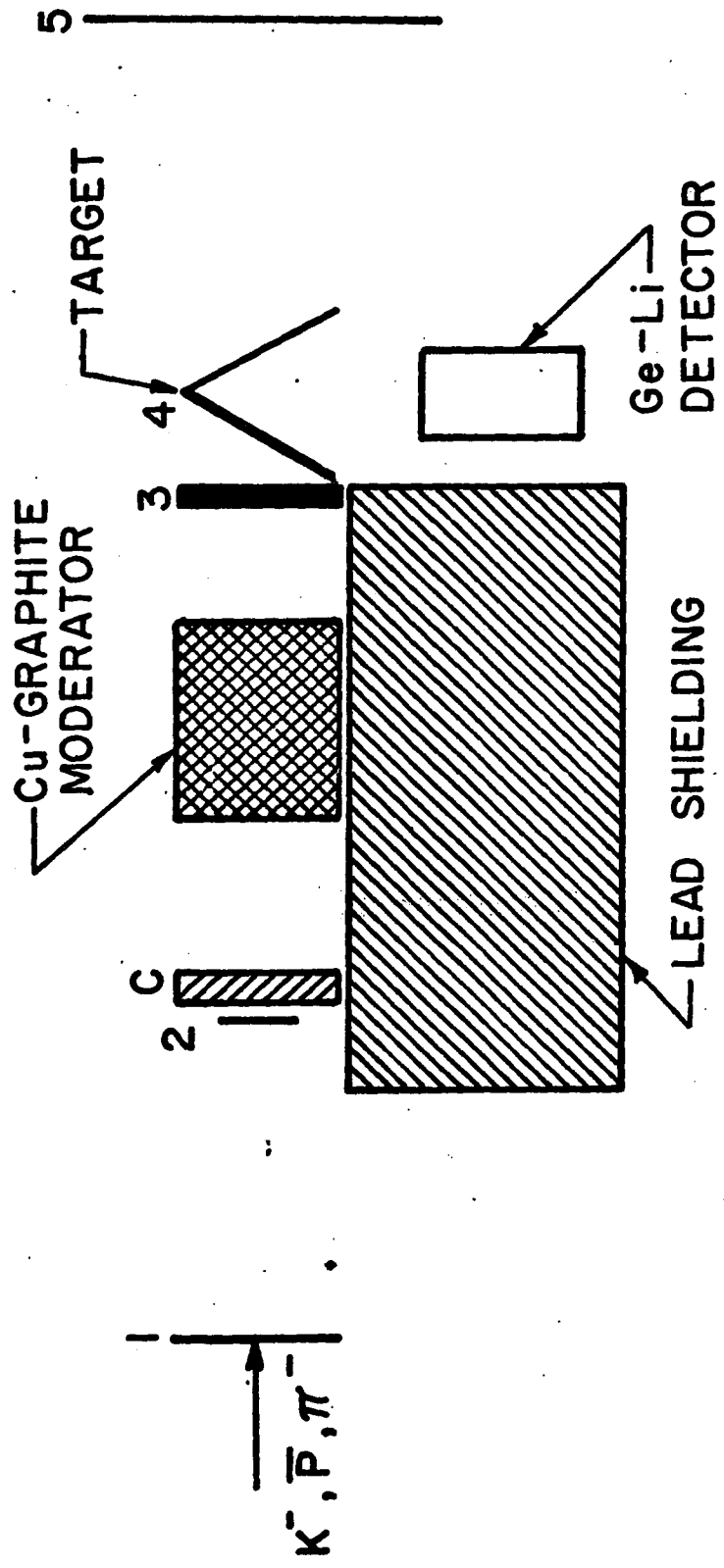


FIG. 2



COUNTER GEOMETRY

FIG. 3

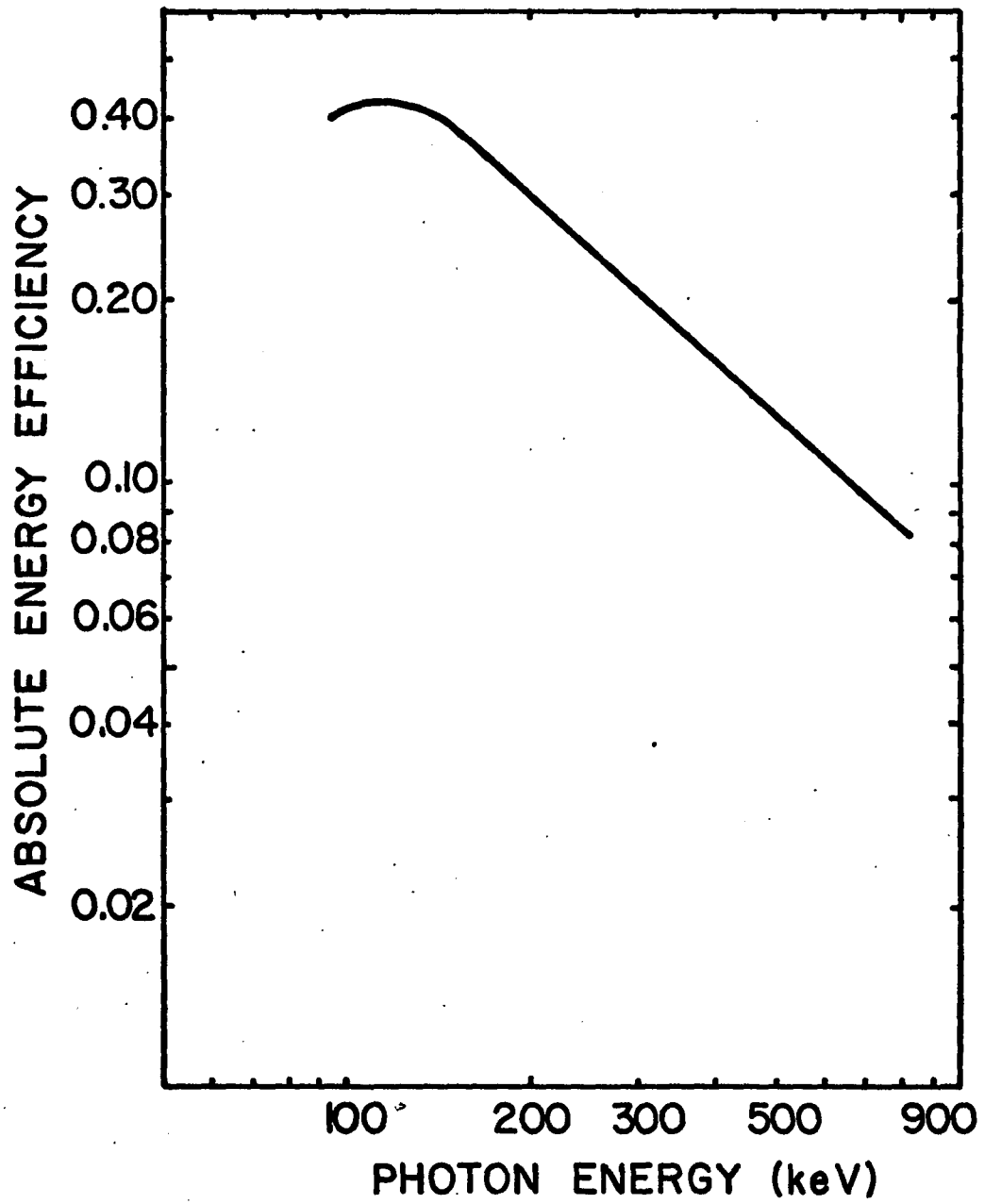


FIG. 4

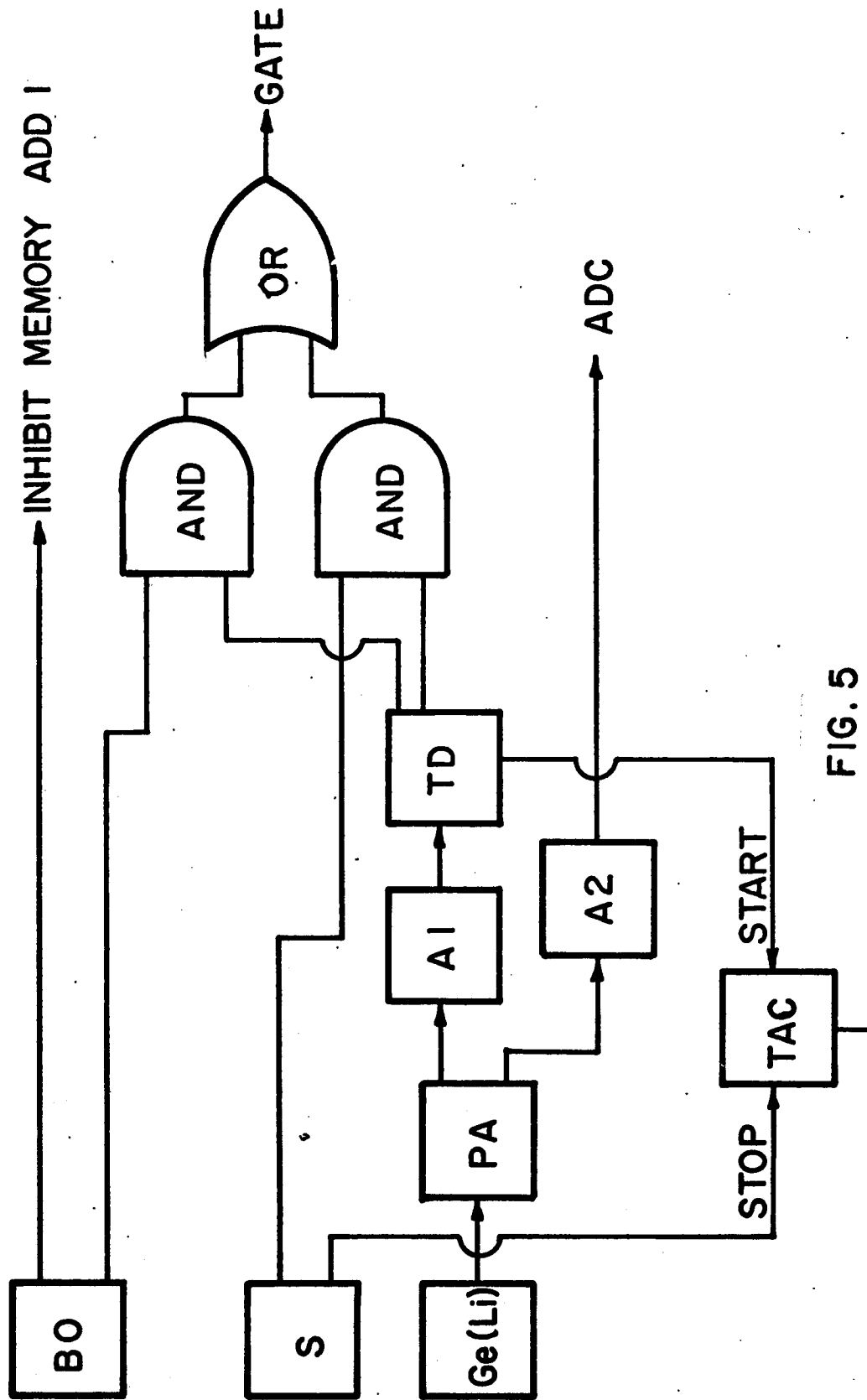
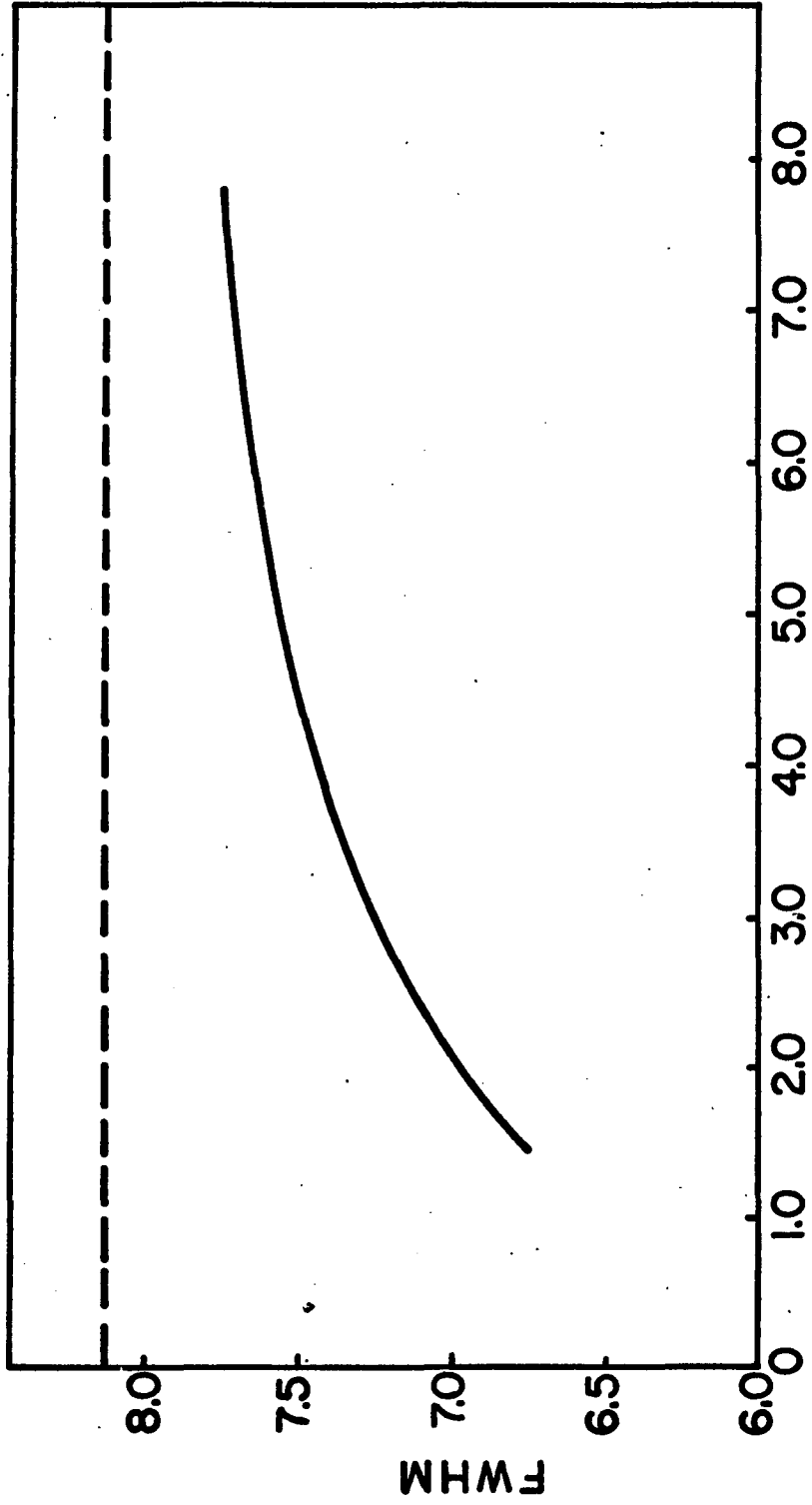


FIG. 5



R (CIRCULAR / NON-CIRCULAR)

FIG. 6

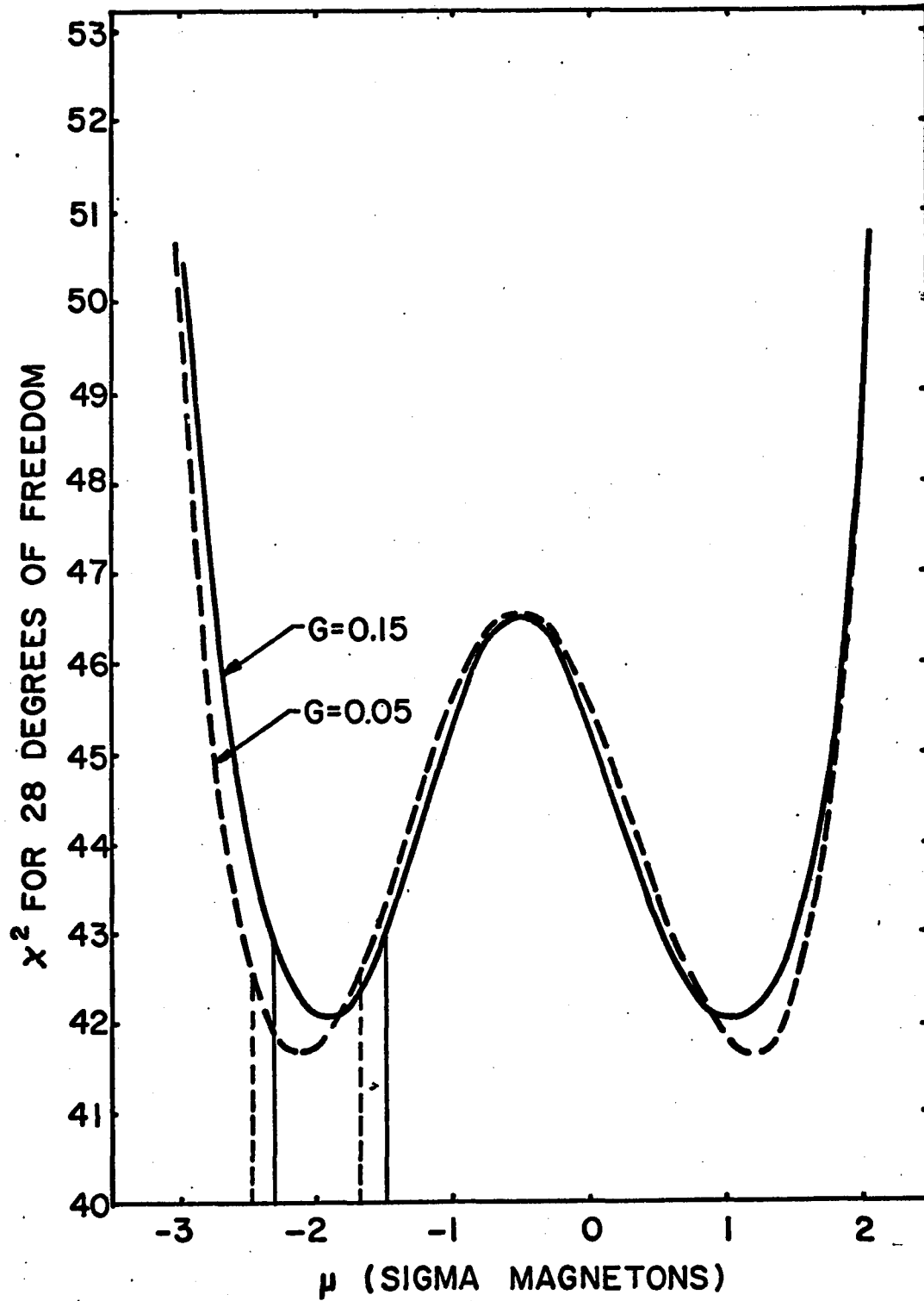


FIG. 7

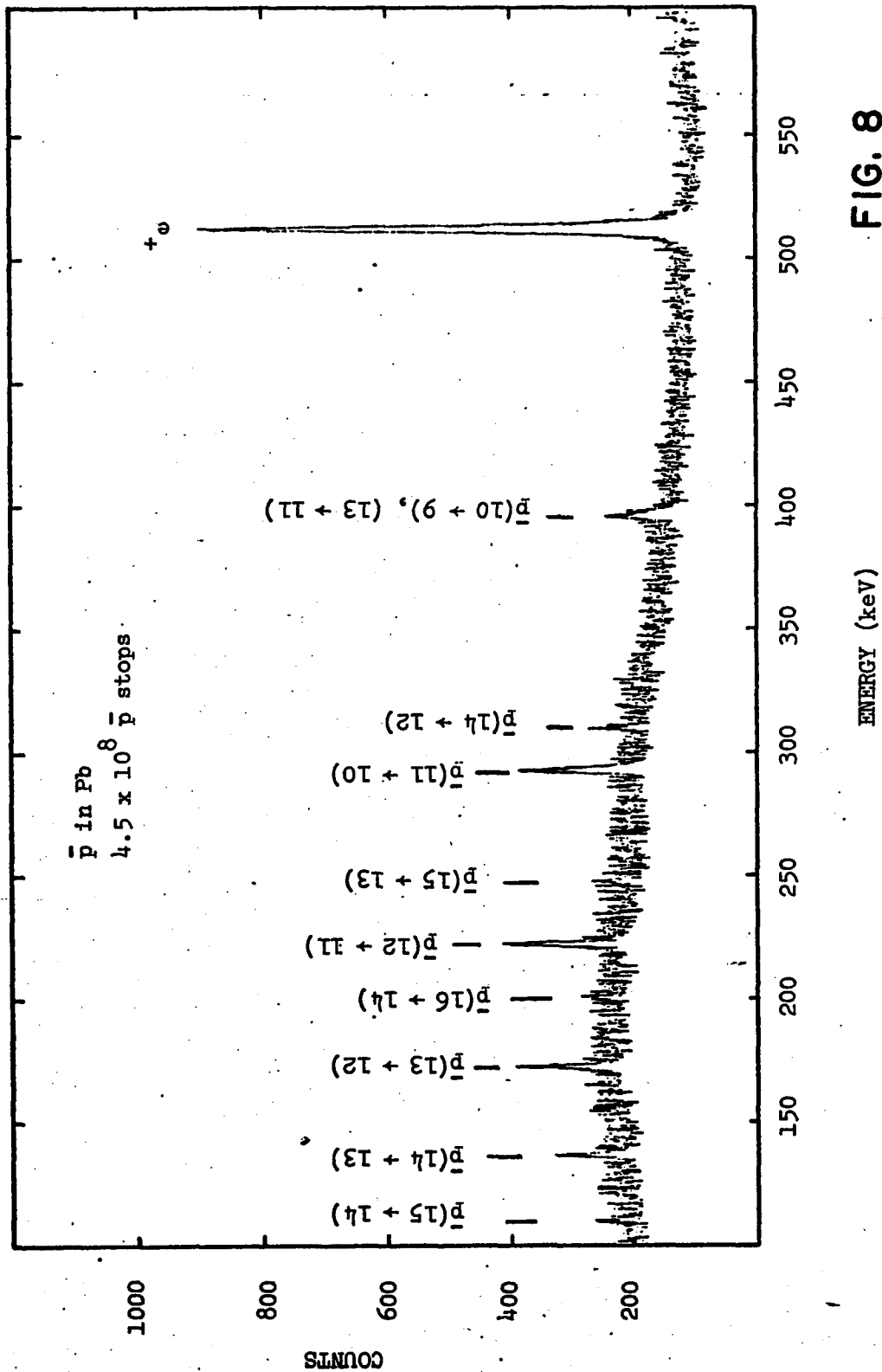


FIG. 8

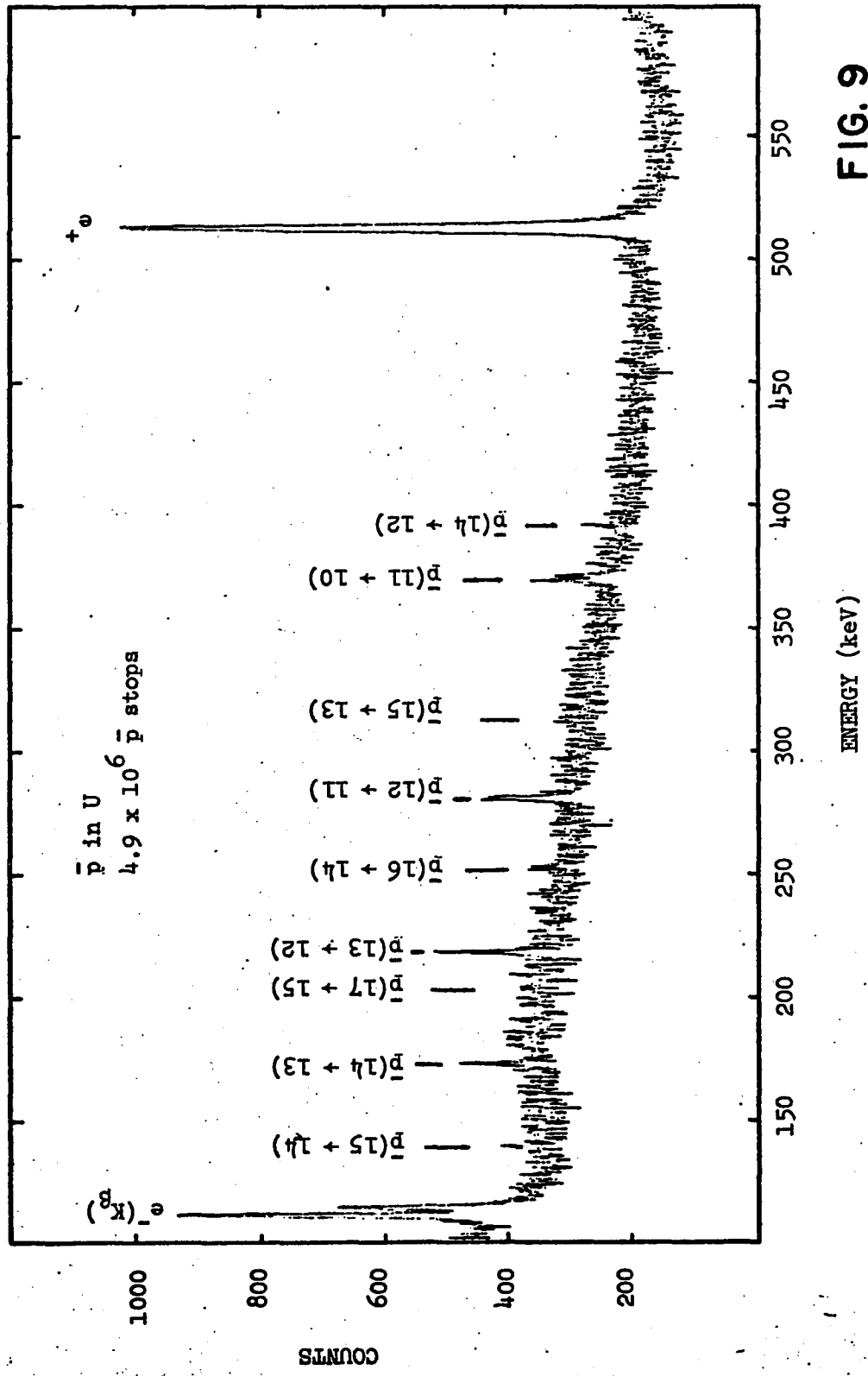


FIG. 9

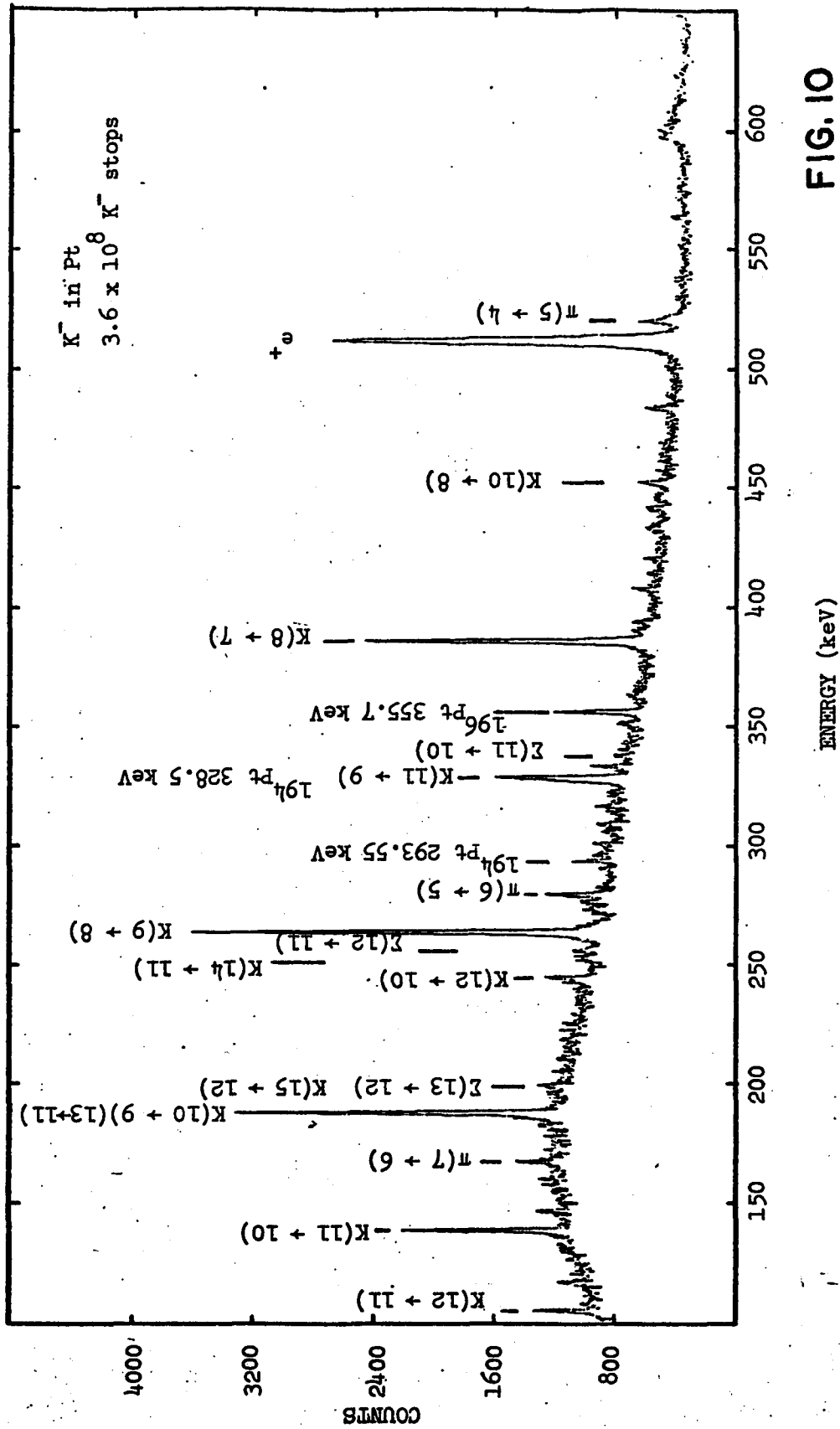


FIG. 10

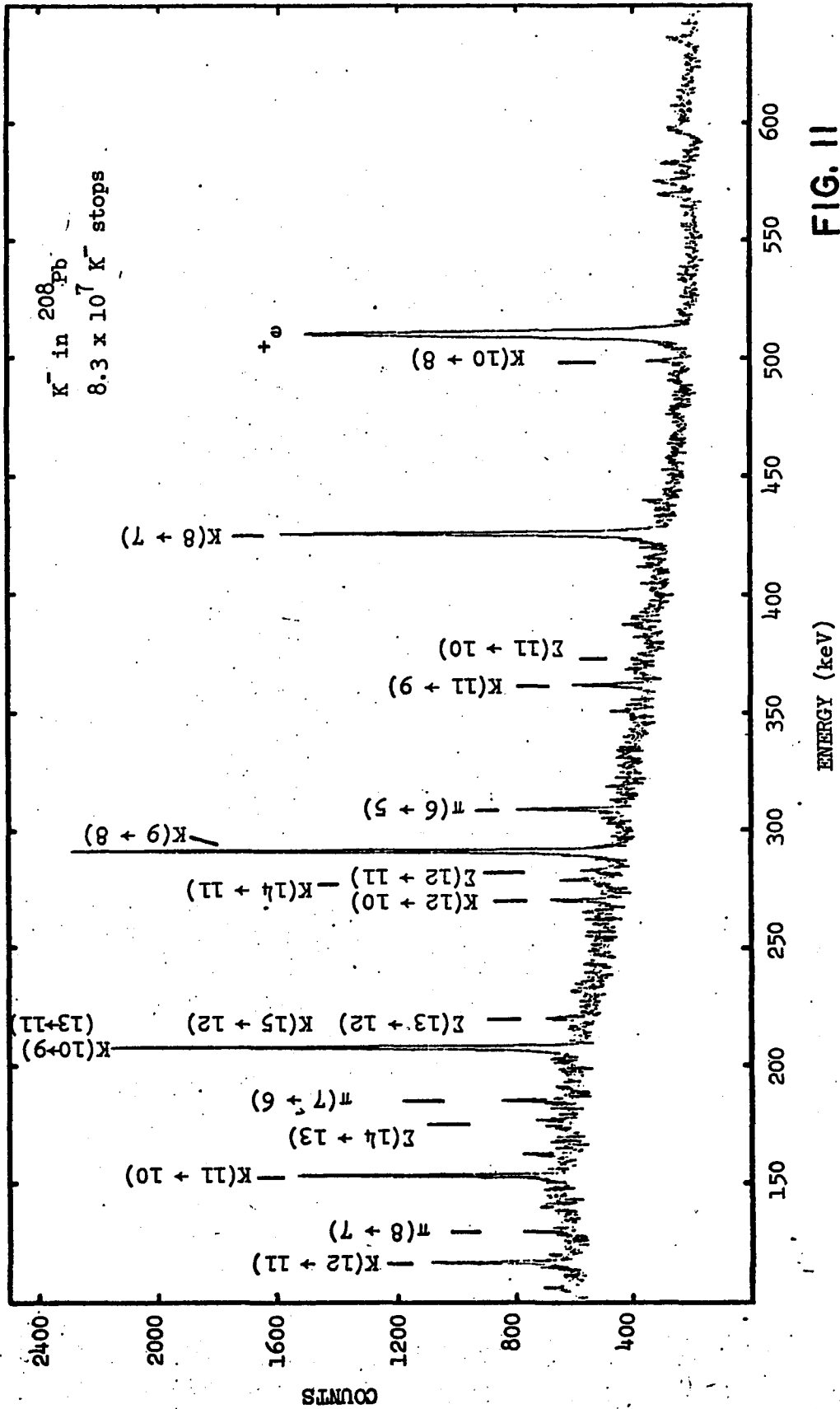


FIG. II

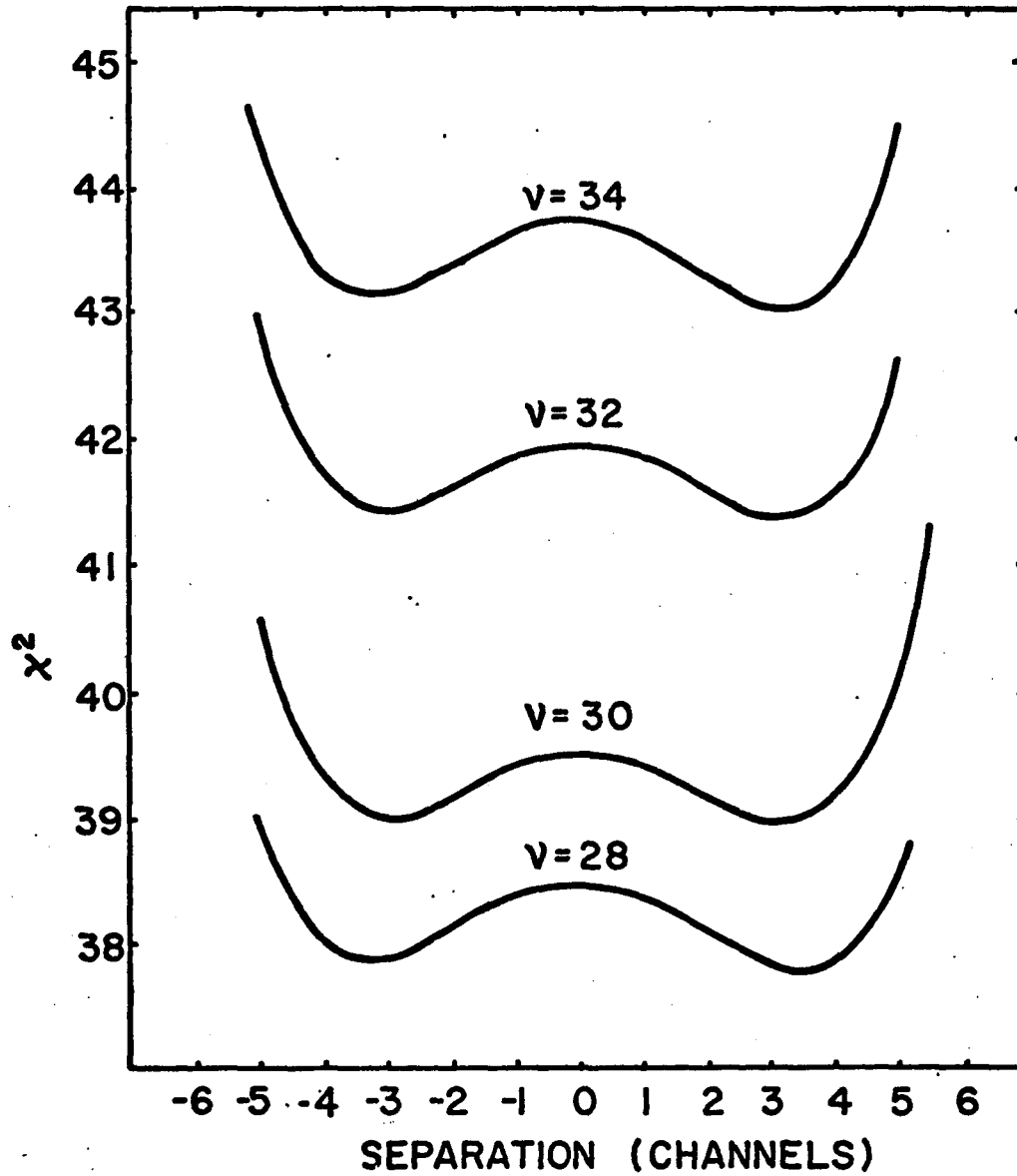


FIG. 12

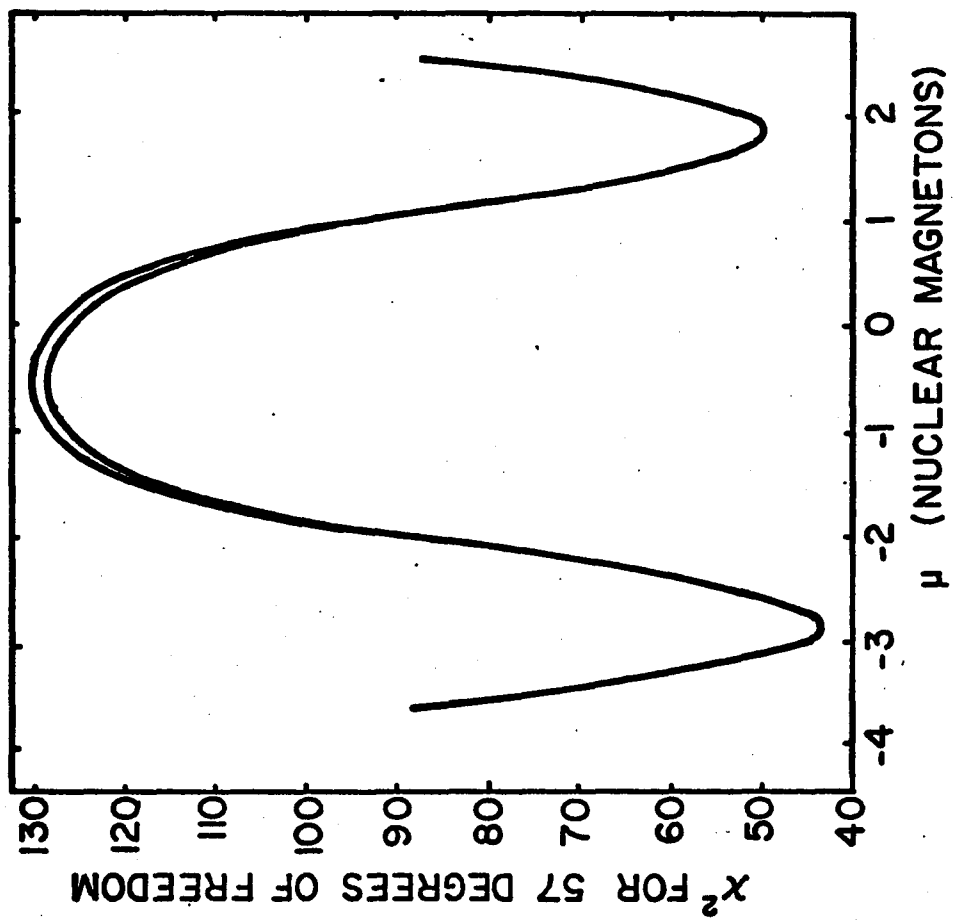


FIG. 13

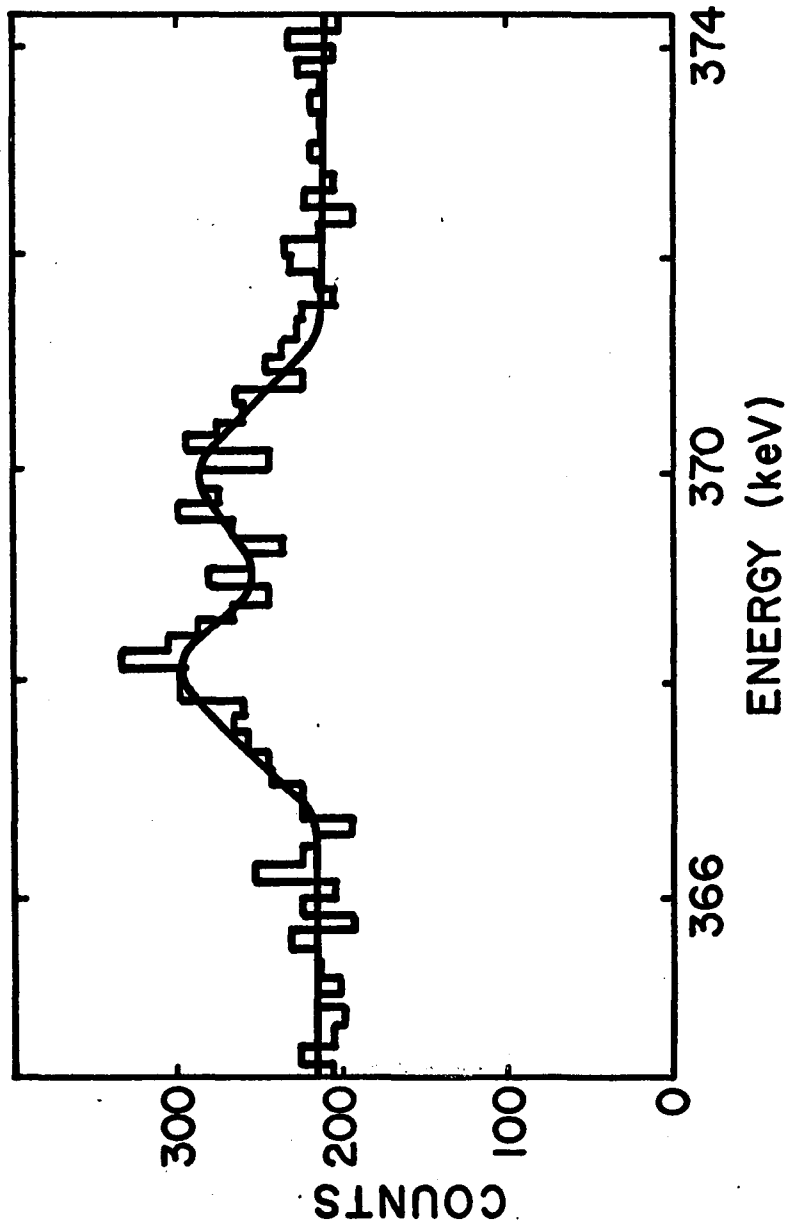


FIG. 14

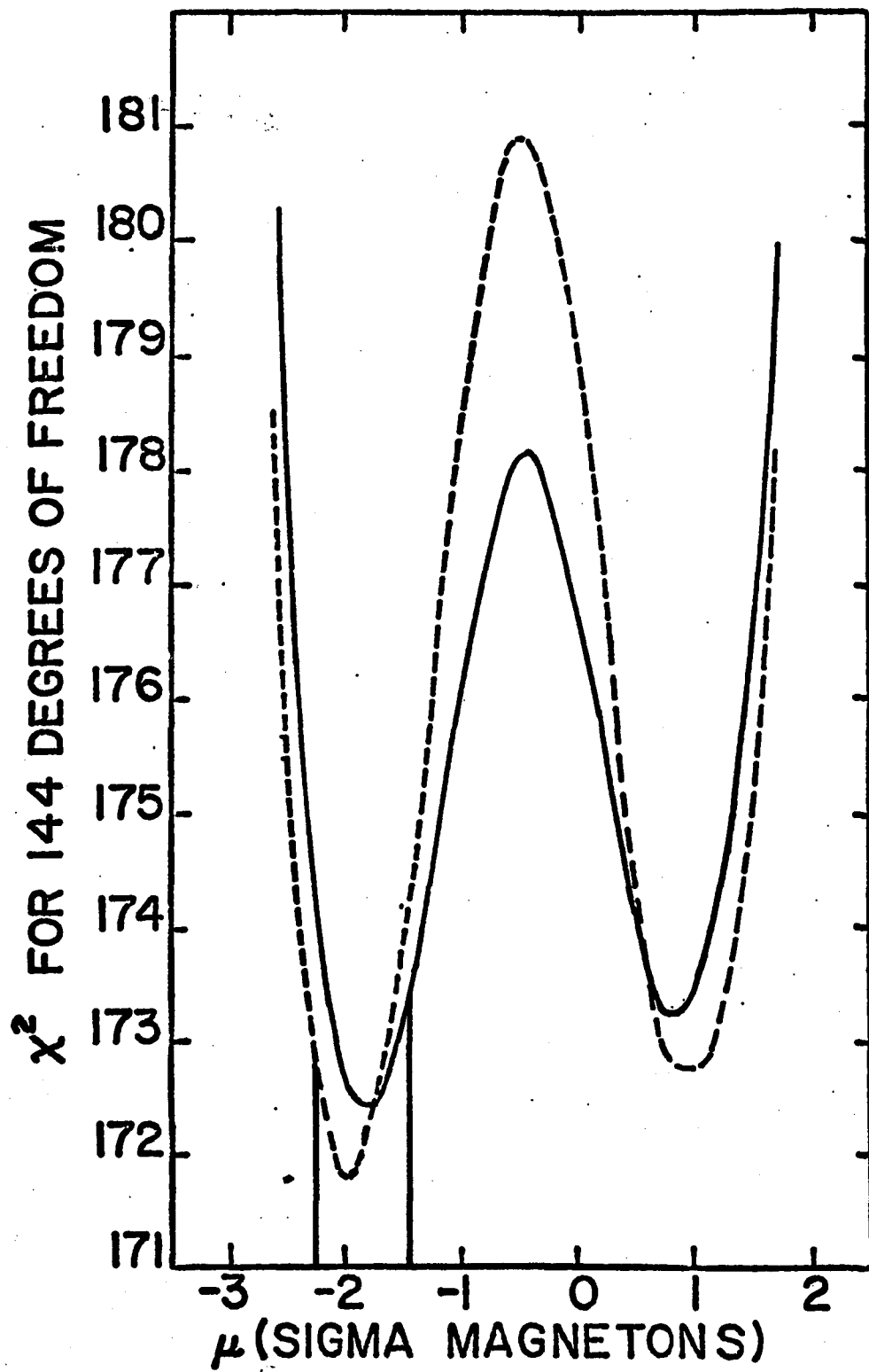


FIG. 15